Neurobiology of Disease

A Distinct Metabolically Defined Central Nucleus Circuit Bidirectionally Controls Anxiety-Related Behaviors

Jing Ren,[1*] Cheng-Lin Lu,[1*] Jie Huang,[2] Jun Fan,[1] Fang Guo,[1] Jia-Wen Mo,[1] Wei-Yuan Huang,[1] Peng-Li Kong,[1] Xiao-Wen Li,[1] Li-Rong Sun,[1] Xiang-Dong Sun,[2] and Xiong Cao[1,3,4]

[1]Key Laboratory of Mental Health of the Ministry of Education, Guangdong-Hong Kong-Macao Greater Bay Area Center for Brain Science and Brain-Inspired Intelligence, Guangdong Province Key Laboratory of Psychiatric Disorders, Department of Neurobiology, School of Basic Medical Sciences, Southern Medical University, Guangzhou 510515, People's Republic of China, [2]School of Basic Medical Sciences, Institute of Neuroscience and Department of Neurology, Second Affiliated Hospital of Guangzhou Medical University, Guangzhou 510260, People's Republic of China, [3]Microbiome Medicine Center, Department of Laboratory Medicine, Zhujiang Hospital, Southern Medical University, Guangzhou 510515, People's Republic of China, and [4]Department of Psychology, School of Public Health, Southern Medical University, Guangzhou 510515, People's Republic of China

Anxiety disorders are debilitating psychiatric diseases that affect ~16% of the world's population. Although it has been proposed that the central nucleus of the amygdala (CeA) plays a role in anxiety, the molecular and circuit mechanisms through which CeA neurons modulate anxiety-related behaviors are largely uncharacterized. Soluble epoxide hydrolase (sEH) is a key enzyme in the metabolism of polyunsaturated fatty acids (PUFAs), and has been shown to play a role in psychiatric disorders. Here, we reported that sEH was enriched in neurons in the CeA and regulated anxiety-related behaviors in adult male mice. Deletion of sEH in CeA neurons but not astrocytes induced anxiety-like behaviors. Mechanistic studies indicated that sEH was required for maintaining the the excitability of sEH positive neurons (sEH^{CeA} neurons) in the CeA. Using chemogenetic manipulations, we found that sEH^{CeA} neurons bidirectionally regulated anxiety-related behaviors. Notably, we identified that sEH^{CeA} neurons directly projected to the bed nucleus of the stria terminalis (BNST; $sEH^{CeA–BNST}$). Optogenetic activation and inhibition of the $sEH^{CeA–BNST}$ pathway produced anxiolytic and anxiogenic effects, respectively. In summary, our studies reveal a set of molecular and circuit mechanisms of sEH^{CeA} neurons underlying anxiety.

Key words: **anxiety; CeA; CeA-BNST pathway; soluble epoxide hydrolase**

Significance Statement

Soluble epoxide hydrolase (sEH), a key enzyme that catalyzes the degradation of EETs, is shown to play a key role in mood disorders. It is well known that sEH is mostly localized in astrocytes in the prefrontal cortex and regulates depressive-like behaviors. Notably, sEH is also expressed in central nucleus of the amygdala (CeA) neurons. While the CeA has been studied for its role in the regulation of anxiety, the molecular and circuit mechanism is quite complex. In the present study, we explored a previously unknown cellular and circuitry mechanism that guides sEH^{CeA} neurons response to anxiety. Our findings reveal a critical role of sEH in the CeA, sEH^{CeA} neurons and CeA-bed nucleus of the stria terminalis (BNST) pathway in regulation of anxiety-related behaviors.

Received July 30, 2021; revised Jan. 18, 2022; accepted Jan. 21, 2022.

Author contributions: J.R. and X.C. designed research; J.R., C.-L.L., J.H., J.F., F.G., J.-W.M., W.-Y.H., P.-L.K., X.-W.L., L.-R.S., X.-D.S., and X.C. performed research; J.R., C.-L.L., J.H., X.-D.S., and X.C. analyzed data; J.R. wrote the first draft of the paper; X.-D.S. edited the paper; J.R. and X.C. wrote the paper.

This work was supported by the National Natural Science Foundation of China (31771187, 81801293), the Guangzhou Science and Technology Project (201904020039, 202007030013), the National Program for Support of Top-notch Young Professionals, The Key Area Research and Development Program of Guangdong Province (2018B030334001, 2018B030340001), the Natural Science Foundation of Guangdong (2020B1515020006) and the Program for Changjiang Scholars and Innovative Research Team in University (IRT_16R37). We thank Xin-Hong Zhu (Southern Medical University) for providing *Ephx2*$^{loxp/loxp}$ and *Ephx2-iCreER*^{T2} mice. We also thank Wen-Chao Xiong, Ying-Ying Fang, Shu-Ji Li, Ting Guo, and Rong-Qing Chen (Southern Medical University) for their technical support.

*J.R. and C.-L.L. contributed equally to this work.

The authors declare no competing financial interests.

Correspondence should be addressed to Xiong Cao at caoxiong@smu.edu.cn or Xiang-Dong Sun at xisun@gzhmu.edu.cn.

https://doi.org/10.1523/JNEUROSCI.1578-21.2022

Introduction

Anxiety disorders, which have a global lifetime prevalence of ~16%, rank as a leading cause of disability and global disease burden and are the most common and debilitating psychiatric disorder (Mnookin, 2016; World Health Organization, 2017; Huang et al., 2019; Purves et al., 2020). However, the mechanism of anxiety disorders remains elusive. Evidence from human, primate and rodent studies has implicated that the central nucleus of the amygdala (CeA) plays a critical for the pathogenesis of anxiety disorders. (Kalin et al., 2004; Tye et al., 2011; Birn et al., 2014; Calhoon and Tye, 2015; Gilpin et al., 2015; Tovote et al., 2015; Ahrens et al., 2018; Dedic et al., 2018; Pomrenze et al., 2019; Griessner et al., 2021). Whereas, the CeA-related molecular mechanism and neural circuits involved in anxiety remain incompletely explored.

The brain is highly enriched with polyunsaturated fatty acids (PUFAs; Bazinet and Layé, 2014), especially arachidonic acid (ARA), which has been implicated in the regulation of mood disorders, such as anxiety disorders and depression (Nery et al., 2008; Kim et al., 2011; Mocking et al., 2013). ARA is metabolized to the biologically active product eicosanoid through cyclooxygenase, lipoxygenase and cytochrome P450. The P450 epoxygenase pathway metabolizes ARA to hydroxyeicosatetraenoic acids (n-HETEs) and epoxyeicosatrienoic acids (EETs; Harris and Hammock, 2013; Morisseau and Hammock, 2013; Atone et al., 2020). Soluble epoxide hydrolase (sEH), a key enzyme that catalyzes the degradation of EETs, is involved in anorexia nervosa and mood disorders (Scott-Van Zeeland et al., 2014; Ren et al., 2016; Lee et al., 2019; Xiong et al., 2019). In the prefrontal cortex, sEH is mostly localized in astrocytes and regulates depressive-like behaviors (Marowsky et al., 2009; Xiong et al., 2019). Intriguingly, sEH is suggested to be expressed in neurons in the CeA region (Marowsky et al., 2009). However, the detailed expression pattern of sEH in the CeA and its functions are still unknown.

Here, we found that deletion of sEH in CeA neurons promoted anxiety-like behaviors. Mechanistic studies showed that inhibition of sEH, deletion of sEH both reduced the excitability of sEH-positive neurons in the CeA (sEH^{CeA} neurons). Furthermore, combining chemogenetic methods, viral tracing and optogenetics, we dissected the functional organization of the sEH^{CeA} neurons which then drove downstream targets in the bed nucleus of the stria terminalis (BNST) to modulate anxiety-related behaviors. Taken together, we uncover a previously unknown cellular and circuitry mechanism underlying CeA-involved modulation of anxiety-related behaviors.

Materials and Methods

Animals

All animal protocols were approved by the Southern Medical University Animal Ethics Committee. All experiments were performed on adult male mice (8–16 weeks old). Mice were housed in groups (three to five per cage) and under controlled temperature (22–25°C) conditions in a 12/12 h light/dark cycle (lights on from 7 A.M. to 7 P.M.) with *ad libitum* access to food and water. Male C57BL/6J mice (aged 8–12 weeks) were obtained from the Southern Medical University Animal Center (Guangzhou, China).

The loxp-flanked *Ephx2* mouse line ($Ephx2^{loxp/loxp}$) was generated as described in our previous report (Xiong et al., 2019). *Ephx2-iCreER*^{T2} mice were constructed in Shanghai Model Organisms Center (Shanghai, China). This model was generated by CRISPR/Cas9 inserting 2A-CreERT2 at the termination codon of the *ephx2* gene (MGI: 99500) through homologous recombination. The donor vector, constructed by In-Fusion cloning, included a 4.822 kb 5′ homologous arm, 2A-CreERT2 and a 4.909 kb 3′ homologous arm. Cas9 mRNA, gRNA and donor vector were microinjected into the germ cells of C57BL/6J mice to obtain F0 pups. F0 mice were genotyped with the following primers: forward: 5′-CCGAGGCTGAACTGGAGAAGA-3′ and reverse: 5′-CAGCATTTGTGAACAGAAGGGTC-3′. According to the PCR results, the targeted F0 mice were identified. F0 mice were backcrossed with C57BL/6J mice to obtain F1 mice. The F1 pups were screened for the desired mutant allele using prior genomic PCR genotyping. The *Ephx2-iCreER*^{T2} mice were genotyped with the following primers: 5′-TCTGCCCCGCTCAGGTCT-3′, 5′-ATGGCACAGGCATACTCAAA-3′, and 5′-TTCCAGGTATGCTCAGAAAACG-3′. The expected PCR products were one band with 342 bp for wild-type, two bands with 342 and 369 bp for heterozygous and one band with 369 bp for homozygous animals. *Cre*-dependent ROSA26-tdTomato reporter mouse lines (The Jackson Laboratory catalog #007909, RRID: IMSR_JAX:007909) were purchased from The Jackson Laboratory. *Ephx2*-tdTomato mice were generated by crossing *Ephx2-iCreER*^{T2} mice with ROSA26-tdTomato mice. In order to excise the loxp sites by Cre recombination, two-month-old male mice (*Ephx2*-tdTomato and *Ephx2-iCreER*^{T2} mice) were intraperitoneally injected with tamoxifen (TAM; Sigma-Aldrich catalog #T5648) once a day (100 mg kg^{-1}) for 5 d. TAM was dissolved in corn oil (Sigma-Aldrich catalog #C8267) at a final concentration of 10 mg ml^{-1}. For fiber photometry recording and chemogenetic and optogenetic experiments, TAM was injected 7 d after virus injection. For immunofluorescence, experiments were performed one month after TAM injection. Behavioral tests were conducted on three- or four-month-old male mice studied 30 d or 60 d after the first TAM injection.

All mice were handled per day for 3–4 d before the behavioral experiments, and double-blind behavioral tests were performed between 1 and 4 P.M.

Viruses

The viruses AAV2/9-hSyn-DIO-GCaMP6s-WPRE-pA (viral: 2.09×10^{12} vg ml^{-1}), AAV2/9-hSyn-DIO-hM3D(Gq)-mCherry-WPRE-pA (viral: 7.37×10^{12} vg ml^{-1}), AAV2/9-hSyn-DIO-hM4D(Gi)-mCherry-WPRE-pA (viral: 2.63×10^{12} vg ml^{-1}), AAV2/9-Ef1α-DIO-hChR2(H134R)-EYFP-WPRE-pA (viral: 5.48×10^{12} vg ml^{-1}), AAV2/9-Ef1α-DIO-eNpHR3.0-mCherry-WPRE-pA (viral: 3.25×10^{12} vg ml^{-1}) and AAV2/9-GFAP-CRE-GFP (viral: 2.4×10^{12} vg ml^{-1}) were purchased from BrainVTA (Wuhan, China). The virus AAV2/9-hSyn-FLEX-mGFP-2A-synaptophysin-mRuby (viral: 3.8×10^{12} vg ml^{-1}) and AAV2/2Retro-hEf1α-DIO-EYFP-WPRE-pA (viral: 1.26×10^{13} vg ml^{-1}) was provided by Taitool Bioscience.

The shRNA sequences targeting *Ephx2* (GenBank accession: NM_007940) were 5′- GCAGCTGATTGGAGAGTAA-3′. A negative control (NC) sequence (TTCTCCGAACGTGTCACGT) was used as the control shRNA. The specificity and efficiency of the shRNAs were validated, and the engineered AAV (AAV-*Ephx2*-shRNA, 1.0×1011 vg ml^{-1}) and AAV2/9-hSyn-Cre-eGFP- WPRE-pA (viral: 3.59×10^{13} vg ml^{-1}) were produced by Obio Technology Corp. Ltd.

Cannula implantation/virus injection/optical fiber implantation

For pharmacological experiments, a unilateral or bilateral cannula (RWD Life Science) was implanted into the CeA [anteroposterior (AP): −1.06; mediolateral (ML): ±2.8; dorsoventral (DV): −4.4; mm relative to bregma] for infusion of 2 μl sEH inhibitor TPPU at a rate of 1 μl min^{-1} (1 μM, Sigma-Aldrich, catalog #SML0750, CAS: 1222780-33-7). The cannula and screws were held in place with dental cement. Mice were allowed to recover for one week after implantation. All behavioral tests were performed 30 min after the infusion.

Mice were anesthetized with sodium pentobarbital (50 mg kg^{-1}, i.p.) for bilateral or unilateral stereotaxic injection of viruses into the CeA (AP: −1.06; ML: ±2.8; DV: −4.6; mm relative to bregma). The coordinates were measured from the bregma according to the mouse atlas. A volume of 300-nl virus was injected into each location at a rate of 100 nl min^{-1}. After each injection, the needle was left in place for 6 min and then slowly withdrawn.

For fiber photometry, a ceramic ferrule with an optical fiber [200 μm in diameter, numerical aperture (NA) of 0.37 (Inper)] was implanted with the fiber tip on top of the CeA (bregma −1.06 mm, lateral ±2.8 mm, and dura −4.60 mm) after 30 min of AAV injection. TAM was injected (intraperitoneally) once a day (100 mg kg^{-1}) for 5 d on the eighth day of AAV injection. The GCaMP signals were recorded three weeks after optical fiber implantation. For projection-specific optogenetic manipulations, mice were unilaterally (ChR2) or bilaterally (NpHR) injected with 300 nl of virus into the CeA, and then TAM was injected (intraperitoneally) in the next week. Optic fibers (length 5 mm, NA 0.37; Inper) were implanted over the BNST (AP: +0.14 mm, ML: ±0.9 mm, DV: −4.2 mm) five to seven weeks after virus injection. Behavior tests were conducted 10 d later.

A designer receptor exclusively activated by a designer drug (DREADD)

Ephx2-iCreER^{T2} mice were bilaterally injected with hM3Dq or hM4Di into the CeA following TAM injection one week later. After four weeks of virus expression, mice were injected with clozapine-N-oxide (CNO;

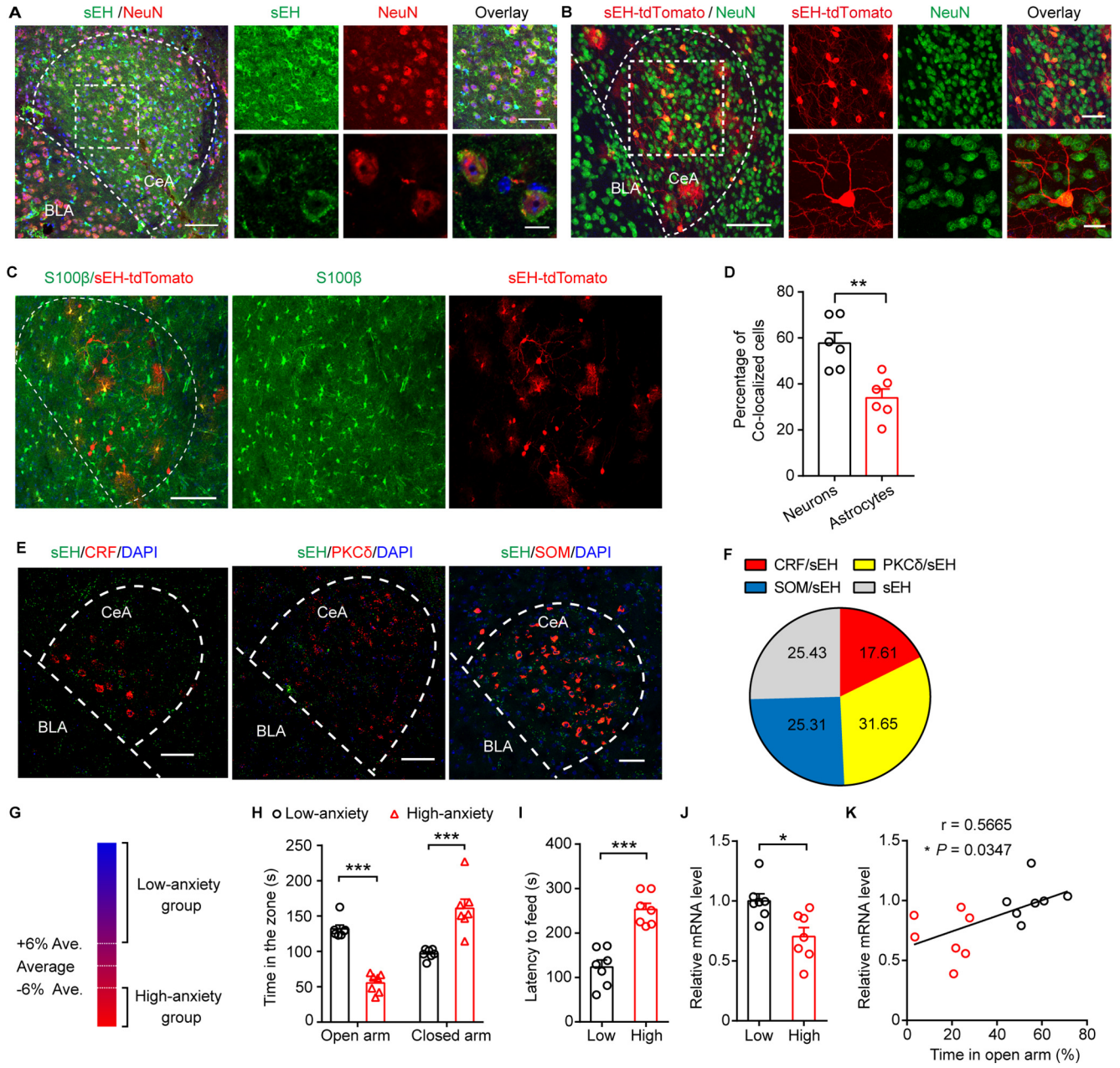

Figure 1. sEH is enriched in neurons in the CeA and is associated with anxiety-related behaviors. ***A***, left, Double immunofluorescence staining with sEH (red) and NeuN (green) reveals co-localization in the CeA of adult C57BL/6J mice. Scale bar: 100 μm. Right, Magnified view of left image. Scale bars: 50 μm (top) and 10 μm (bottom). ***B***, left, Representative images of CeA *Ephx2*(sEH)-tdTomato neurons (red) from the *Ephx2-iCreER*^{T2}; *Ai9* mice co-stained for NeuN (green). Scale bar: 100 μm. Right, Zoomed-out view of left image. Scale bars: 50 μm (top) and 20 μm (bottom). ***C***, Representative images of CeA *Ephx2*(sEH)-tdTomato neurons (red) from the *Ephx2-iCreER*^{T2}; *Ai9* mice co-stained for S100β (green). Scale bar: 100 μm. ***D***, Percentage of sEH^{+} neurons in the CeA that co-express NeuN and S100β ($t = 4.025$, $^{**}p = 0.0024$, $n = 6$ slices from 3 mice). ***E***, Single-molecule fluorescence *in situ* for sEH (green) and the indicated alternate cell markers-CRF (red), PKCδ (red), and SOM (red) in the CeA of C57 mice. Scale bars: 50 μm. ***F***, Percentage of sEH^{+} neurons in the CeA that co-express CRF, PKCδ, and SOM ($n = 3$ sections per mouse, 3 mice per marker). ***G***, Experimental design for identification of the high-anxiety and low-anxiety mice. ***H***, Mice are divided into high-anxiety and low-anxiety subgroups in the EPM according to ***G***. Time in the open arm, $t_{(12)} = 10.42$, $^{***}p < 0.0001$; time in the closed arm, $t_{(12)} = 4.874$, $^{***}p = 0.0004$. ***I***, After the EPM test, the mice were screened again with the NSF according to ***G***. $t_{(12)} = 6.25$, $^{***}p < 0.0001$. ***J***, Real-time quantitative fluorescence PCR analysis shows CeA sEH mRNA expression in high-/low-anxiety mice. $t_{(12)} = 3.052$, $^{*}p = 0.0101 < 0.05$. ***K***, Correlations between the sEH mRNA level and the time in open arms (%) of low-anxiety and high-anxiety mice. Pearson correlation coefficient, $r = 0.5665$, $^{*}p = 0.0101 < 0.05$. Data are presented as the mean ± SEM. Two-tailed unpaired Student's *t* test, NS ≥ 0.05; $^{*}p \leq 0.05$, $^{***}p \leq 0.001$, $^{****}p \leq 0.0001$.

2 mg/kg, i.p.; Sigma-Aldrich, catalog #C0832, CAS: 34233-69-7) and placed into the test room to habituate for 60 min. Stimulation-induced behaviors were scored manually by a human observer inspecting the videos *post hoc* (EthoVision by Noldus) while blinded to the underlying conditions.

Fiber photometry recording

GCaMP6s virus injection and optic fiber implantation were performed on *Ephx2*-tdTomato mice (approximately eight weeks old) on the same day. Fiber optic calcium recording was conducted three weeks after virus injection. A fiber photometry system (Thinker Tech) was used for recording GCaMP signals from genetically identified neurons. To induce fluorescence signals, a laser beam from a laser tube (488 nm) was reflected by a dichroic mirror, focused by a ×10 (NA of 0.3) lens and coupled to an optical commutator. The GCaMP6s fluorescence was bandpass filtered (MF525-39, Thorlabs) and collected by a photomultiplier tube (R3896, Hamamatsu). An amplifier (C7319, Hamamatsu) was

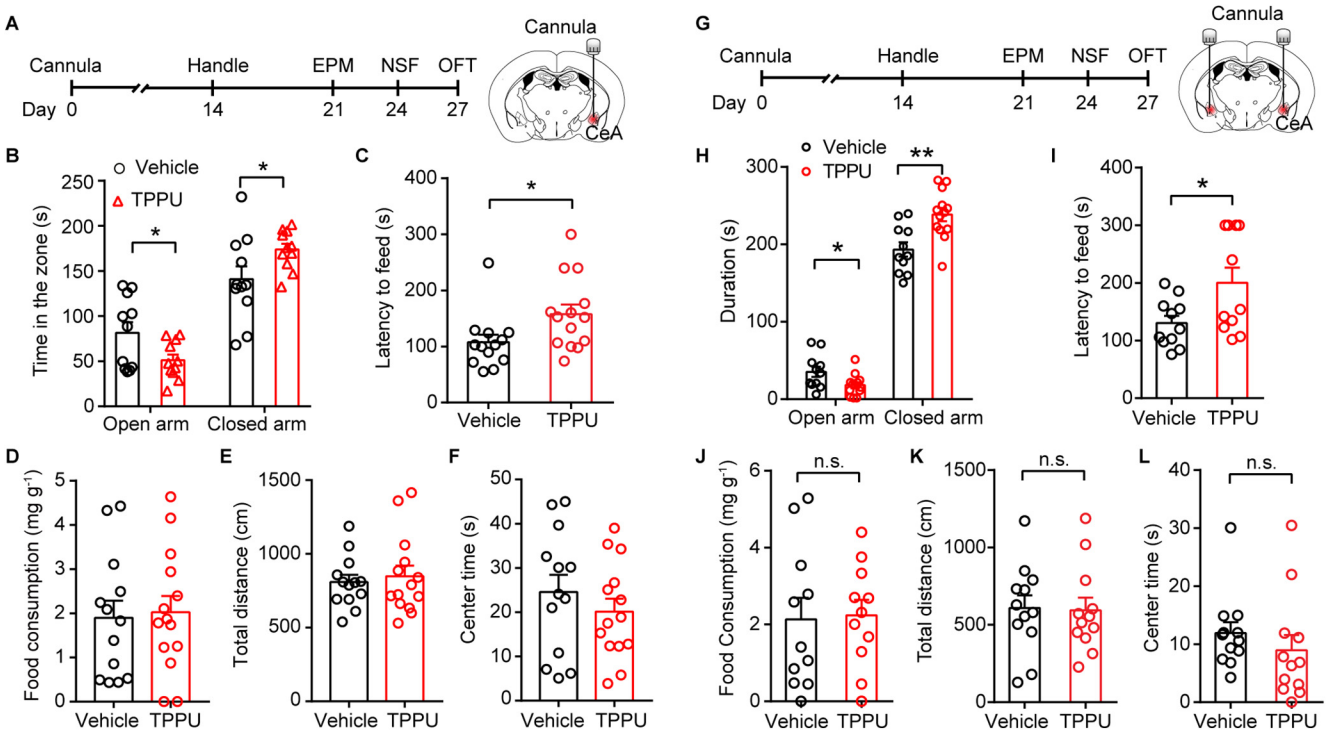

Figure 2. Infusion of sEH inhibitor in CeA induces anxiety-like behaviors. ***A***, Schematic of the unilateral drug administration and behavior tests. ***B***, ***C***, EPM and NSF tests for adult C57BL/6J mice treated with the sEH inhibitor TPPU (1 μM) or vehicle unilaterally. Time in the open arm, $t_{(20)} = 2.235$, $^{*}p = 0.037 < 0.05$; time in the closed arm, $t_{(20)} = 2.103$, $^{*}p = 0.0483$ (***B***); $t_{(25)} = 2.263$, $^{*}p = 0.0326 < 0.05$, $n = 13$ for vehicle mice, $n = 14$ for TPPU mice (***C***). ***D***, Food consumption during the NSF test for adult C57BL/6J mice treated with the sEH inhibitor TPPU (1 μM) or vehicle unilaterally. $t_{(25)} = 0.2355$, $p = 0.8157$, $n = 13$ for vehicle mice, $n = 14$ for TPPU mice. ***E***, ***F***, OFT for adult C57BL/6J mice treated with TPPU or vehicle unilaterally. $t_{(25)} = 0.4462$, $p = 0.6593$ (***E***); $t_{(25)} = 0.9121$, $p = 0.3704$, $n = 13$ for vehicle mice, $n = 14$ for TPPU mice (***F***). ***G***, Schematic of the bilateral drug administration and behavior tests. ***H***, ***I***, EPM and NSF tests for adult C57BL/6J mice treated with the sEH inhibitor TPPU (1 μM) or vehicle bilaterally. Time in the open arm, $t_{(22)} = 2.355$, $^{*}p = 0.0278 < 0.05$; time in the closed arm, $t_{(22)} = 3.56$, $^{**}p = 0.0018 < 0.01$ ($n = 11$ for vehicle mice, $n = 13$ for TPPU mice; ***H***); $t_{(20)} = 2.409$, $^{*}p = 0.0258 < 0.05$ (***I***). ***J***, Food consumption during the NSF test for adult C57BL/6J mice treated with the sEH inhibitor TPPU (1 μM) or vehicle bilaterally. $t_{(20)} = 0.1515$, $p = 0.8811 > 0.05$. ***K***, ***L***, OFT for adult C57BL/6J mice treated with TPPU or vehicle bilaterally. $t_{(20)} = 0.1208$, $p = 0.9049$ (***K***); $t_{(20)} = 0.9123$, $p = 0.3715 > 0.05$ (***L***). Data are presented as the mean ± SEM. Two-tailed unpaired Student's *t* test, NS ≥ 0.05; $^{*}p \leq 0.05$, $^{***}p \leq 0.001$, $^{****}p \leq 0.0001$.

used to convert the photomultiplier tube current output to voltage signals, which were further filtered through a low-pass filter (40-Hz cutoff; Brownlee 440). A flashing light-emitting diode triggered by a 1-s square-wave pulse was simultaneously recorded to synchronize the video and GCaMP signals. To minimize photobleaching, the power intensity at the fiber tip was adjusted to 30 μW. For recordings in freely moving mice, mice with optical fibers connected to the fiber photometry system were freely explored in the elevated plus maze (EPM) for 5 min. After the experiments, the optical fiber tip sites were histologically examined in each mouse. Calcium signals for the bulk fluorescence signals were acquired and analyzed with custom-written MATLAB software. The Z-score of a population of neurons was calculated using the formula: $Z = (x\text{-}y)/SD$ (where $x = F_{Signal}$, y = mean of $F_{Baseline}$, and SD for standard deviation of $F_{Baseline}$).

Optogenetic manipulations

An optical fiber was initially implanted into the BNST in the brain of an anesthetized mouse that had been immobilized in a stereotaxic apparatus. The implant fiber was secured to the animal's skull with dental cement. Chronically implantable fibers (diameter, 200 μm, Inper) were connected to a laser generator using optic fiber sleeves. The delivery of blue light (470 nm, 10–15 mW, 5-ms pulses, 20 Hz) or yellow light (580 nm, 5–10 mW, constant) was controlled by a stimulator. The same stimulus protocol was applied in the control group. The location of the fiber was examined after all the experiments, and data obtained from mice in which the fibers were outside the desired brain region were discarded.

Brain slice electrophysiology

Mice were anesthetized with isoflurane and perfused with 15- to 20-ml regular artificial CSF (ACSF) containing the following: 126 mM NaCl, 3 mM KCl, 1 mM $MgSO_4$, 2 mM $CaCl_2$, 1.25 mM NaH_2PO_4, 26 mM $NaHCO_3$, and 10 mM glucose. The brain was then quickly removed and chilled in ice-cold modified ACSF containing the following: 120 mM choline chloride, 2.5 mM KCl, 7 mM $MgCl_2$, 0.5 mM $CaCl_2$, 1.25 mM NaH_2PO_4, 25 mM $NaHCO_3$, and 10 mM glucose. Coronal brain slices were cut in ice-cold modified ACSF using a VT-1000S vibratome (Leica) and quickly transferred to an incubation chamber containing regular ACSF at 32°C for 30 min and at room temperature (25 ± 1°C) for an additional 1 h before recording. All liquids were saturated with 95% O_2/5% CO_2 (v/v).

The brain slices were placed in the recording chamber, with continuous perfusion of ACSF at a flow rate of 2 ml min^{-1}. Whole-cell patch-clamp recording from neurons in the CeA region was visualized with infrared optics using an upright microscope equipped with an infrared-sensitive charge-coupled device (CCD) camera (DAGE-MTI, IR-1000E). The pipettes were pulled by a micropipette puller (P-97, Sutter Instrument) with a resistance of 3–5 MΩ. Recordings were made with a MultiClamp 700B amplifier and 1440A digitizer (Molecular Device).

To detect the excitability of CeA neurons, the APs were recorded under the current-clamp mode by injecting a series of gradually increased depolarizing pulses starting from 0 to 80 pA at a step of 20 pA, with the pipette solution including the following: 125 mM Glu-K, 5 mM KCl, 10 mM HEPES, 0.2 mM EGTA, 1 mM $MgCl_2$, 4 mM MgATP, 0.3 mM NaGTP, and 10 mM Na_2-phosphocreatine (pH 7.40, 285 mOsm). The resting membrane potential was considered the value without current injection, and the membrane input resistance was calculated in response to a series of hyperpolarizing pulses.

For the drug treatment experiments, slices from *Ephx2*-tdTomato mice were incubated with drugs (TPPU, 1 μM; 11,12-EET, 2 μM,

Cayman Chemical, catalog #50511) or vehicle for 30 min and then subjected to recording.

In all experiments, cells were rejected if the series resistance was larger than 20 MΩ during the recordings or if the series resistance fluctuated by >20% of the initial values. Data were filtered at 1 kHz and sampled at 10 kHz.

Real-time quantitative PCR

Total RNA was obtained from cells or tissues using RNAiso plus (TaKaRa) according to the manufacturer's instructions and was quantified with a Nanodrop 2000 (Thermo Scientific). cDNA was synthesized using the PrimeScript RT Reagent kit (Takara). Quantitative real-time PCR was performed in an ABI 7500 Real-Time PCR System with SYBR premix Ex Taq (TaKaRa). The ΔΔCt method was used to analyze gene expression, and relative mRNA levels were normalized to 18s mRNA levels. The *Ephx2* primer sequences were as follows: forward primer, GGACGACGGAGAC AAGAGAG; reverse primer, CTGTGTTGTGGA CCAGGATG.

Western blot analysis

Mouse brain tissue from the CeA was homogenized in lysis buffer (RIPA) on ice for 30 min and subsequently centrifuged at 12,000 rpm for 20 min at 4°C. Supernatants were transferred to a clean 1.5-ml tube, and samples containing 80 μg of protein were separated using 10% SDS-PAGE gels. Proteins were electrotransferred onto PVDF membranes in ice-cold buffer (25 mM Tris HCl, 192 mM glycine, and 20% methanol) over the course of 2 h. The membranes were blocked with 5% nonfat milk powder dissolved in TBST. The membranes were incubated overnight at 4°C with monoclonal rabbit anti-sEH (1:1000, Shanghai YouKe) and polyclonal mouse anti-GAPDH (1:10,000, Proteintech Group, catalog #60004-1-Ig, RRID: AB_2107436). HRP-conjugated goat anti-mouse and goat anti-rabbit secondary antibodies were purchased from ABclonal (AS014, AS003). Protein abundance was quantified by analyzing the Western blot bands using AlphaEaseFC (WB) software. Quantification of band intensities was normalized to GAPDH and averaged from at least three independent experiments.

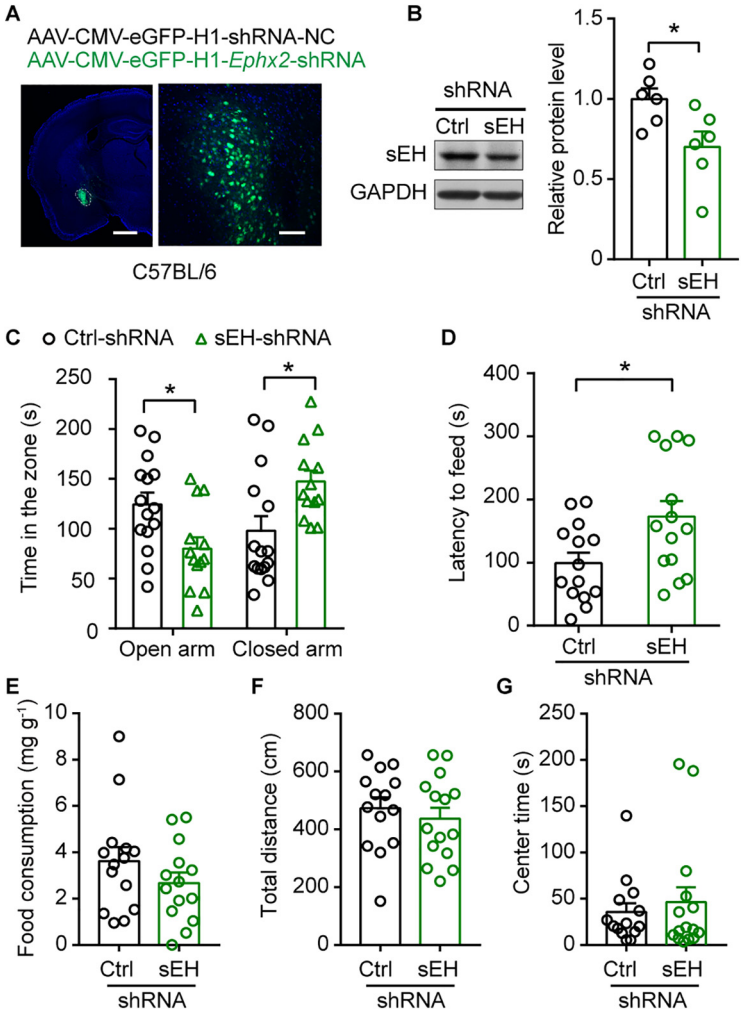

Figure 3. KD of sEH in the CeA produces anxiety-like behaviors. ***A***, Expression of AAV-*Ephx2*-shRNA in the CeA of adult C57BL/6J mice. Scale bar: 1000 μm (left) and 100 μm (right). ***B***, Left, Western blotting representation of sEH protein levels in the CeA after infection with shRNA or control virus. Right, Quantification of sEH protein levels in the CeA after infection with shRNA or control virus. $t_{(10)} = 2.572$, $^{*}p = 0.0278 < 0.05$. ***C***, ***D***, EPM and NSF tests for adult C57BL/6J mice bilaterally CeA injected with shRNA or control virus. Time in the open arm, $t_{(26)} = 2.666$, $^{*}p = 0.013$; time in the closed arm, $t_{(26)} = 2.638$, $^{*}p = 0.0139 < 0.05$ ($n = 15$ for control mice, $n = 13$ for shRNA mice; ***C***); $t_{(26)} = 2.502$, $^{*}p = 0.019 < 0.05$ (***D***). ***E***, Food consumption during the NSF test for adult C57BL/6J mice bilaterally CeA injected with AAV-*Ephx2*-shRNA or control virus. $t_{(26)} = 1.246$, $p = 0.224 > 0.05$. ***F***, ***G***, OFT for adult C57BL/6J mice bilaterally injected with AAV-*Ephx2*-shRNA or control virus. $t_{(27)} = 0.6703$, $p = 0.5084$ (***F***); $t_{(27)} = 0.5522$, $p = 0.5853 > 0.05$ (***G***; $n = 14$ for control mice, $n = 15$ for shRNA mice). Data are presented as the mean ± SEM. Two-tailed unpaired Student's *t* test, NS ≥ 0.05; $^{*}p \leq 0.05$, $^{***}p \leq 0.001$, $^{****}p \leq 0.0001$.

Immunofluorescence

Animals were deeply anesthetized with sodium pentobarbital (50 mg kg^{-1}, i.p.) and perfused transcardially with saline followed by 4% PFA in 0.1 M PBS, pH 7.4. Brains were removed, postfixed overnight in 4% PFA at 4°C and transferred to 30% sucrose in 0.1 M PBS, pH 7.4. Coronal sections (40 μm) were cut on a freezing microtome (Leica CM3050 S) and stored in 0.1 M PBS. In some instances, immunoreactivity was increased by incubating the slices in 10 mM Sodium citrate, 0.05% Tween 20, pH 6 for 10 min at 95°C. The sections were incubated in blocking buffer containing1% bovine serum albumin or 10% donkey serum in 0.3% Triton X-100/PBS for 2 h at room temperature and then with primary antibodies in blocking buffer overnight at 4°C. The primary antibodies used were sEH (1:500, Shanghai Youke Biotechnology Co, Ltd.), NeuN (1:300, Millipore, catalog #MAB377, RRID: AB_2298772), S100β (1:200, Abcam, catalog #ab52642, RRID: AB_882426), corticotropin-releasing factor (CRF; 1:1000, Sigma, catalog #C5348, RRID: AB_258893), and protein kinase C δ (PKCδ; 1:500, BD Biosciences, catalog #610398, RRID: AB_397781), and SST(SOM) (1:500, Santa Cruz, catalog #sc-7819, RRID: AB_2302603; Haubensak et al., 2010; Lemos et al., 2012; Onorati et al., 2014). After three washes with PBS, sections were incubated with either Alexa Fluor 488-conjugated or Alexa Fluor 594/568-conjugated secondary antibodies at room temperature for 2 h. After another three washes in PBS, sections were incubated with Vectashield mounting medium containing DAPI (Vector Laboratories Inc.) and immunofluorescence was assessed using a Nikon A1R confocal microscope (Nikon Instruments Inc.).

RNAscope in situ *hybridization*

The fixed frozen brain slices (10 μm thick) containing CeA were prepared as described above. We performed single-molecule fluorescence *in situ* hybridization using RNAscope fluorescence detection assays and probes (Advanced Cell Diagnostics: RNAscope Probe-Mm-Ephx2 #558701; RNAscope Probe-Mm-Prkcd-C2 #441791-C2; RNAscope Probe -Mm-Sst-C2 #404631-C2; RNAscope Probe-

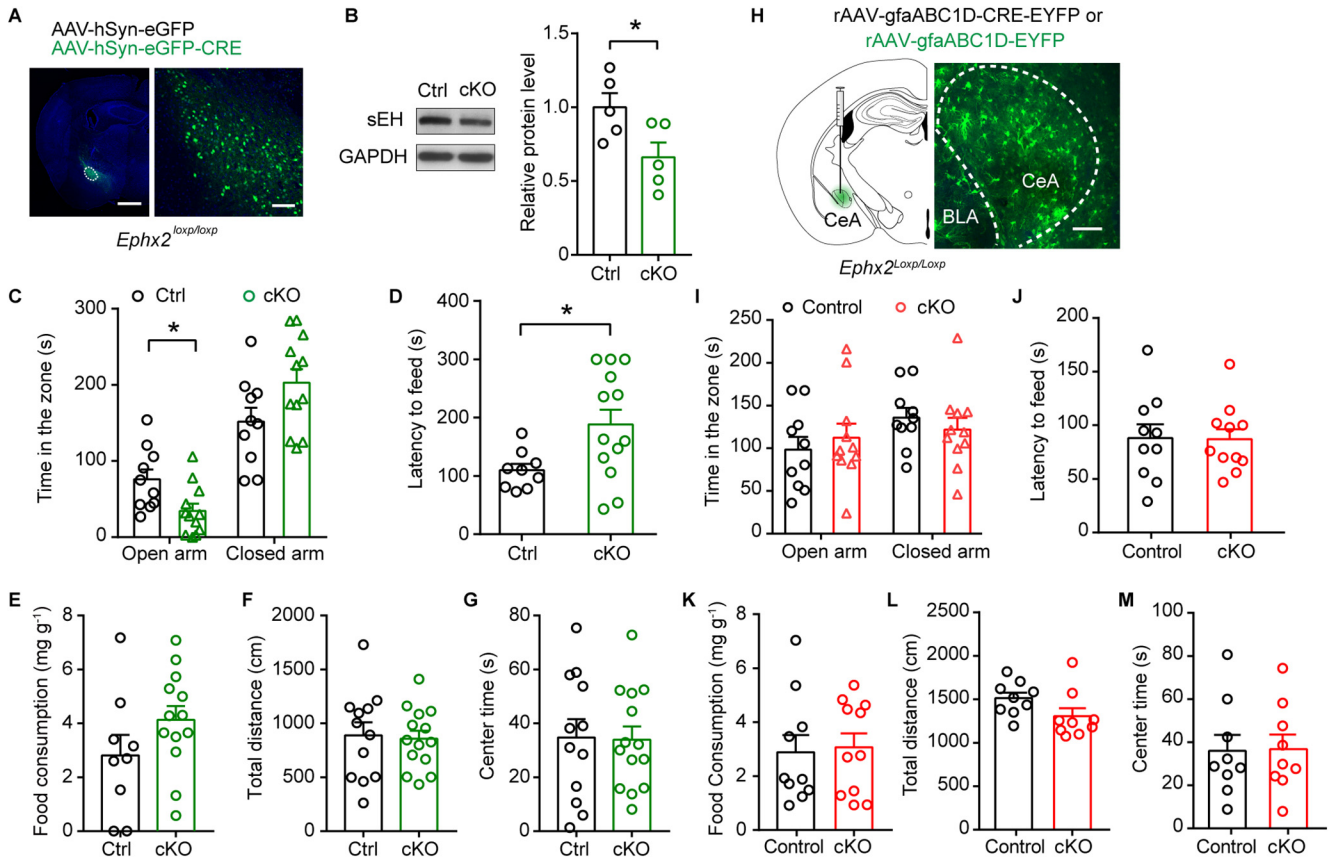

Figure 4. Conditional knock-out of sEH in the CeA neurons results in anxiety-like behaviors. ***A***, Expression of AAV-hSyn-cre virus in the CeA of adult *Ephx2*$^{loxp/loxp}$ mice. Scale bar: 1000 μm (left) and 100 μm (right). ***B***, left, Western blotting representation of sEH protein levels in the CeA after infection with Syn-cre or control virus. Right, Quantification of sEH protein levels in the CeA after infection with Syn-cre or control virus. $t_{(5)} = 2.46$, $^{*}p = 0.0393 < 0.05$. ***C***, ***D***, EPM and NSF tests for the *Ephx2*$^{loxp/loxp}$ mice bilaterally CeA injected with Syn-cre or control virus. Time in the open arm, $t = 2.625$, $^{*}p = 0.0162$; time in the closed arm, $t = 1.997$, $p = 0.0596$ ($n = 10$ for control mice, $n = 12$ for cKO mice; ***C***); $t = 2.447$, $^{*}p = 0.0238 < 0.05$ (***D***; $n = 9$ for control mice, $n = 13$ for cKO mice). ***E***, Food consumption during the NSF test for the *Ephx2*$^{loxp/loxp}$ mice bilaterally CeA injected with Syn-cre or control virus. $t = 1.496$, $p = 0.1504$ ($n = 9$ for control mice, $n = 13$ for cKO mice). ***F***, ***G***, OFT for *Ephx2*$^{loxp/loxp}$ mice bilaterally CeA injected with syn-cre or control virus. $t = 0.2382$, $p = 0.8138$ (***F***); $t = 0.09818$, $p = 0.9226 > 0.05$ (***G***; $n = 12$ for control mice, $n = 14$ for cKO mice). ***H***, Expression of AAV-gfaABC1D-cre virus in the CeA of adult *Ephx2*$^{loxp/loxp}$ mice. Scale bar: 100 μm. ***I–M***, EPM,NSF and OFT tests for *Ephx2*$^{loxp/loxp}$ mice bilaterally CeA injected with gfaABC1D-cre (cKO mice) or control virus (control mice). Time in the open arm, $t_{(19)} = 0.6195$, $p = 0.5429$, time in the closed arm, $t_{(19)} = 0.7746$, $p = 0.4481$ (***I***); $t_{(19)} = 0.06{,}975$, $p = 0.9451$ (***J***); $t_{(19)} = 0.2226$, $p = 8262$ (***K***); $n = 10$ for control mice, $n = 11$ for cKO mice; $t_{(16)} = 1.859$, $p = 0.0815$ (***L***); $t_{(16)} = 0.07{,}747$, $p = 0.9392$ (***M***). Data are presented as the mean ± SEM. Two-tailed unpaired Student's *t* test, NS ≥ 0.05; $^{*}p \leq 0.05$, $^{***}p \leq 0.001$, $^{****}p \leq 0.0001$.

Mm-Crh-C2 #422791) in eight- to nine-week-old C57 mice according to the manufacturer's protocols. Slides showing poor staining were not analyzed.

Fluorescence microoptical sectioning tomography (fMOST)

AAV2/9-Ef1α-DIO-EYFP- WPRE-pA was injected into the CeA of *Ephx2-iCreER*^{T2} mice to trace the CeA^{sEH} neuron circuit with fMOST system (OE-bio, Co, Ltd.). The whole-brain precise imaging has been described previously (Lin et al., 2018). Briefly, the GMA-embedded mouse brains were imaged by the fMOST system. Whole-brain imaging, imaging process and reconstruction were performed by OE-bio according to the manufacturer's protocols.

EPM

The EPM apparatus comprised two open arms (30 × 5 × 0.5 cm), two closed arms (30 × 5 × 15 cm), and a central platform (5 × 5 cm) elevated 50 cm above the underlying surface. Mice were placed in the center facing one of the two open arms and allowed to explore for 5 min (except the optogenetic experiments). For the optogenetic experiments, individual mice were connected to the patch cable and allowed 1–5 min in the center for recovery from handling before the 9-min session was initiated. Each session was divided into three alternating 3-min epochs: laser stimulation off, stimulation on, and stimulation off (OFF-ON-OFF epochs). Anxiety-related behavior was assessed by time traveled within the open arms. The duration time in the open and closed arms was tracked and recorded by a video tracking system (EthoVision by Noldus).

Novelty-suppressed feeding test

After 24 h of food deprivation and water available *ad libitum*, mice were placed in a brightly lit open arena (50 × 50 × 50 cm) containing clean wood chip bedding. A filter paper (8 × 8 cm) was placed in the center of the arena, and one familiar food pellet was placed in the center of the filter paper. Mice were removed from their home cage, placed in a holding cage for 60 min before testing and then placed in a corner of the testing arena. For optogenetic experiments, the task was repeated twice on different days for each mouse, counterbalanced for no stimulation (OFF) or light stimulation (ON). The task ended when the mice began to eat the food pellet. The latency to begin a feeding episode was recorded with a video camera suspended above the arena and saved for further analysis (EthoVision by Noldus). Immediately after testing, mice were removed from the arena and placed into their home cage to measure food consumption for 5 min.

Open-field test (OFT)

Mice were placed in an open chamber (Accuscan Instruments) with transparent, plastic walls and allowed to explore freely for 5 min (except the optogenetic experiments). Before the start of the optogenetic experiments, mice were allowed to recover from handling for 1–5 min and then placed in the center of the open field. The OFT consisted of a 9-min

session in which there were three alternating 3-min epochs (OFF-ON-OFF epochs). Behavioral tests were recorded by a video camera. The total distance traveled across a session was analyzed by using Versmax analyzer software.

Statistical analysis

All experiments and data analyses were conducted blindly. The number of experimental replicates (n), t, F, and P are indicated in the text and refers to the number of experimental subjects independently treated in each experimental condition. Statistical comparisons were performed using Graph-Pad Prism and SPSS 20.0 software with appropriate inferential methods. Data are presented as the mean ± SEM. Two-tailed Student's t tests, one-way ANOVA, and two-way ANOVA were used for statistical analyses, and differences were considered to be significant if $p < 0.05$. Significance levels are indicated as follows: $^{*}p < 0.05$, $^{**}p < 0.01$, and $^{***}p < 0.001$.

Results

sEH is enriched in neurons in the CeA and is associated with anxiety-related behaviors

To characterize the expression pattern of sEH in the CeA, we employed a specific antibody for sEH (Xiong et al., 2019) and co-stained with NeuN, a marker for neurons, on brain slices from adult C57BL/6J mice. The immunofluorescence results revealed that sEH was present in part of CeA neurons (Fig. 1*A*). Moreover, we generated the *Ephx2*-tdTomato mice by crossing *Ephx2-iCreER*^{T2} mice (a mouse line expressing Cre recombinase under the control of the promoter *ephx2*, which encodes sEH protein) with Ai9 mice (*Cre*-dependent ROSA26-tdTomato reporter mouse line). We found that ~58% of *Ephx2*-tdTomato (sEH-tdTomato) cells in the CeA co-stained with NeuN, whereas ~34% co-stained with S100β, a marker for astrocytes ($t_{(10)} = 4.025$, $p = 0.0024$, unpaired t test; Fig. 1*B–D*). These results indicate that sEH is enriched in neurons in the CeA. To identify the neuron types that sEH is expressed, we performed fluorescence *in situ* hybridization analysis for mRNA localization. The results showed that sEH colocalized with CRF (17.6 ± 5.5%), Somatostatin (SOM; 25.3 ± 5.1%), or PKCδ (31.6% ± 5.8%), which are the main cell markers of GABAergic neurons in the CeA, respectively (Fig. 1*E*,*F*).

To detect whether sEH in the CeA is involved in anxiety, we subjected adult C57BL/6J mice to the EPM and novelty suppressed feeding test (NSF). Mice was separated into high-anxiety and low-anxiety subgroups based on their anxiety levels [Bi et al., 2015; Fig. 1*G–I*; time in the open arm, $t_{(12)} = 10.42$, $p = 0.000$, time in the closed arm, $t_{(12)} = 4.874$, $p = 0.000$ (Fig. 1*H*); $t_{(12)} = 6.25$, $p = 0.000$; unpaired t test (Fig. 1*I*)]. Real-time quantitative fluorescence PCR analysis showed that sEH mRNA

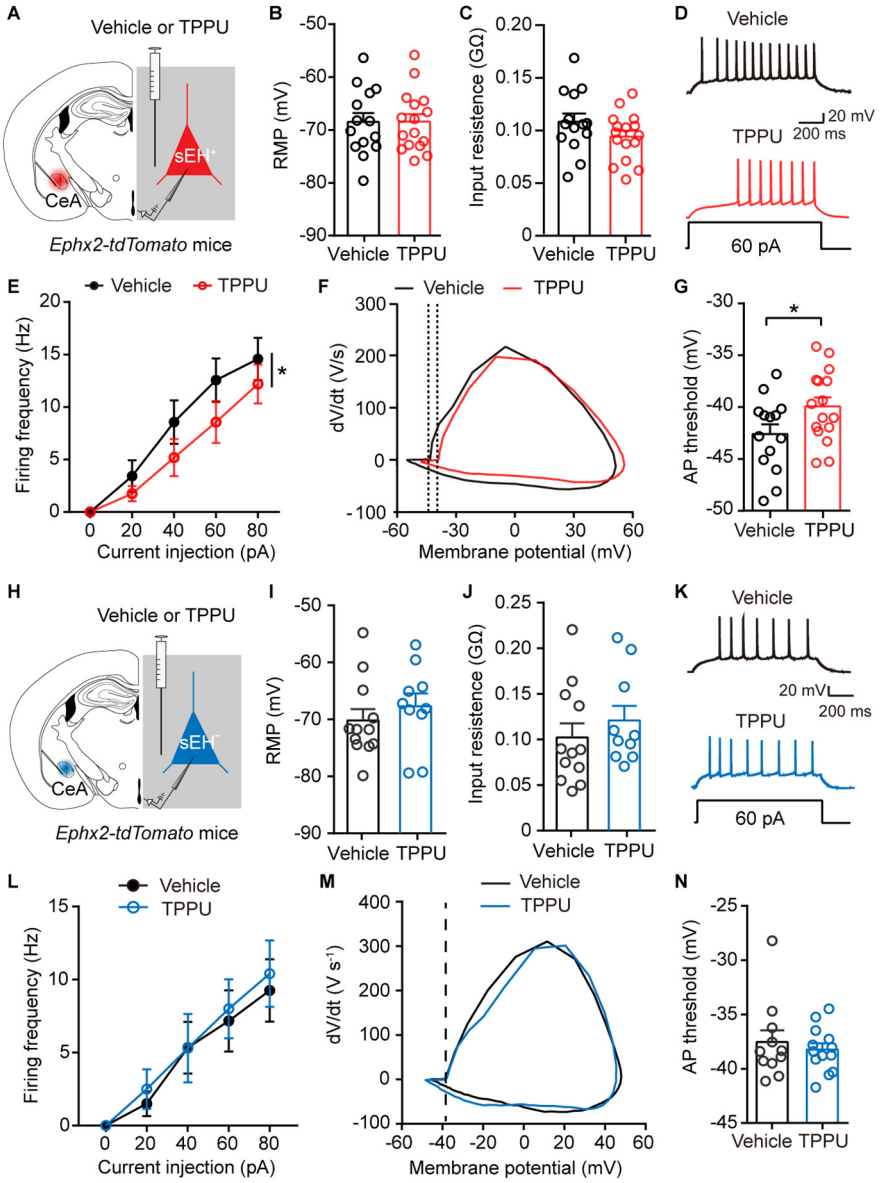

Figure 5. sEH inhibitor TPPU attenuates the intrinsic excitability of sEH-positive neurons in the CeA. ***A,*** Schematic of *in vitro* slice recording in CeA *Ephx2*-tdTomato neurons application with TPPU (sEH inhibitor) or vehicle. ***B***, ***C***, Resting membrane potential and input resistance recorded from *Ephx2*-tdTomato neurons administered the sEH inhibitor TPPU or vehicle. Two-tailed unpaired Student's t test, $t_{(28)} = 0.02999$, $p = 0.9763$ (***B***); $t_{(28)} = 1.467$, $p = 0.1534$ (***C***; vehicle, $n = 14$ cells from 3 mice; TPPU, $n = 16$ cells from 3 mice). ***D***, ***E***, Representative traces of AP responses (***D***) and summarized data (***E***) recorded from *Ephx2*-tdTomato-positive neurons administered TPPU or vehicle. Two-way ANOVA, effect of drug, $F_{(1,140)} = 5.115$, $^{*}p = 0.0253$. ***F***, Phase plots of APs from sEH-positive neurons evoked by brief current injections. ***G***, Plot diagram summary of the AP thresholds from sEH-positive neurons. Two-tailed unpaired Student's t test, $t_{(28)} = 2.098$, $^{*}p = 0.0451 < 0.05$. Vehicle, $n = 14$ cells from 3 mice; TPPU, $n = 16$ cells from 3 mice. ***H***, Schematic of *in vitro* slice recording in CeA *Ephx2*-tdTomato-negative neurons application with TPPU (sEH inhibitor) or vehicle. ***I***, ***J***, Resting membrane potential and input resistance recorded from *Ephx2*-tdTomato-negative neurons treated with TPPU or vehicle. Two-tailed unpaired Student's t test, $t_{(20)} = 0.8129$, $p = 0.4258$ (***I***); $t_{(20)} = 0.8345$, $p = 0.4139$ (***J***; vehicle, $n = 12$ cells from 3 mice; TPPU, $n = 10$ cells from 3 mice). ***K***, ***L***, Representative traces of AP firing (***K***) and summarized data (***L***) recorded from *Ephx2*-tdTomato-negative neurons treated with TPPU or vehicle. Two-way ANOVA, effect of drug, $F_{(1,100)} = 0.2981$, $p = 0.5863$. ***M***, Phase plots of APs from sEH-negative neurons evoked by brief current injections. ***N***, Plot diagram summary of the AP thresholds from sEH-negative neurons. Two-tailed unpaired Student's t test, $t_{(22)} = 0.5923$, $p = 0.5597$ (vehicle, $n = 11$ cells from 3 mice; TPPU, $n = 13$ cells from 3 mice). Data are presented as the mean ± SEM NS ≥ 0.05; $^{*}p \leq 0.05$, $^{***}p \leq 0.001$, $^{****}p \leq 0.0001$.

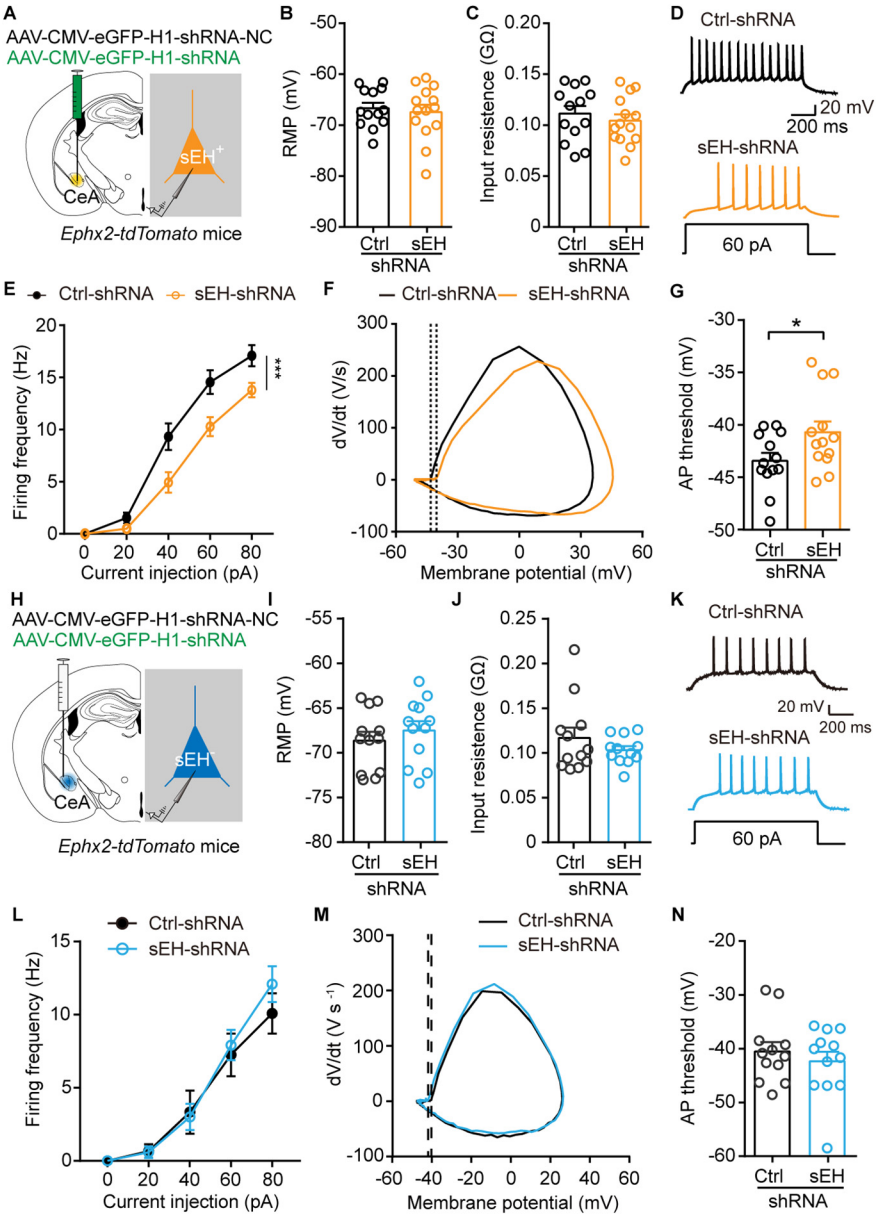

Figure 6. KD of sEH reduces the intrinsic excitability of sEH-positive neurons in the CeA. ***A***, Schematic of *in vitro* slice recording in CeA *Ephx2*-tdTomato neurons after infection with AAV-*Ephx2*-eGFP-shRNA or control virus. ***B***, ***C***, Resting membrane potential and input resistance recorded from *Ephx2*-tdTomato-positive and AAV-*Ephx2*-eGFP-shRNA double-positive neurons. Two-tailed unpaired Student's *t* test, $t_{(25)} = 0.4312$, $p = 0.67$ (***B***); $t_{(25)} = 0.7377$, $p = 0.4676$ (***C***; vehicle, $n = 13$ cells from 3 mice; TPPU, $n = 14$ cells from 3 mice). ***D***, ***E***, Representative traces of AP responses (***D***) and summarized data (***E***). Two-way ANOVA, effect of virus $F_{(1,125)} = 25.84$, $^{***}p < 0.001$. ***F***, Phase plots of APs from Tomato and eGFP double-positive neurons evoked by brief current injections. ***G***, Plot diagram summary of the AP thresholds from Tomato and eGFP double-positive neurons. Two-tailed unpaired Student's *t* test, $t_{(24)} = 2.126$, $^{*}p = 0.044 < 0.05$ ($n = 13$ cells from 3 mice). ***H***, Schematic of *in vitro* slice recording in CeA *Ephx2*-tdTomato-negative neurons in the absence of shRNA virus. ***I***, ***J***, Resting membrane potential and input resistance recorded from *Ephx2*-tdTomato-negative neurons in the absence of shRNA virus. Two-tailed unpaired Student's *t* test, $t_{(22)} = 0.8001$, $p = 0.4322$ (***I***); $t_{(22)} = 1.078$, $p = 0.2929$ (***J***). ***K***, ***L***, Representative traces of AP firing (***K***) and summarized data (***L***) recorded from Tomato-negative neurons in the absence of shRNA virus. Two-way ANOVA, effect of virus, $F_{(1,110)} = 0.5096$, $p = 0.4768$. ***M***, Phase plots of APs from Tomato-negative neurons in the absence of shRNA virus evoked by brief current injections. ***N***, Plot diagram summary of the AP thresholds from Tomato-negative neurons in the absence of shRNA virus. Two-tailed unpaired Student's *t* test, $t_{(22)} = 0.7389$, $p = 0.4678$. Data are presented as the mean ± SEM NS ≥ 0.05; $^{*}p \leq 0.05$, $^{***}p \leq 0.001$, $^{****}p \leq 0.0001$.

expression in the CeA was significantly lower in the high-anxiety subgroup than that in the low-anxiety subgroup ($t_{(12)} = 3.052$, $p = 0.0101$, unpaired *t* test; Fig. 1*J*).More importantly, there was positive and significant correlations between the sEH mRNA level and the time in open arm (%; $r = 0.5665$, $R^2 = 0.3209$, $p = 0.0347$, Pearson *r*; Fig. 1*K*). These results suggest that sEH in the CeA is associated with anxiety-related behaviors.

Neuronal sEH in the CeA modulates anxiety-related behaviors

To investigate the role of sEH in anxiety-related behaviors, we infused the sEH inhibitor 1-(1-propionylpiperidin-4-yl)−3-(4-(trifluoromethoxy)-phenyl)urea (TPPU; 1 μM; Wan et al., 2019) unilaterally or bilaterally into the CeA of adult C57BL/6J mice (Fig. 2*A*,*G*). TPPU treatment significantly reduced the duration of open-arm exploration in the EPM and increased latency to feed in the NSF, without an alteration in food consumption [Fig. 2*B*–*D*,*H*–*J*; time in the open arm, $t_{(20)} = 2.235$, $p = 0.037$, time in the closed arm, $t_{(20)} = 2.103$, $p = 0.0483$ (Fig. 2*B*); $t_{(25)} = 2.263$, $p = 0.0326$; 2D, $t_{(25)} = 0.2355$, $p = 0.8157$ (Fig. 2*C*); time in the open arm, $t_{(22)} = 2.355$, $p = 0.0278$, time in the closed arm, $t_{(22)} = 3.56$, $p = 0.0018$ (Fig. 2*H*); $t_{(20)} = 2.409$, $p = 0.0258$ (Fig. 2*I*); $t_{(20)} = 0.1515$, $p = 0.8811$ (Fig. 2*J*); unpaired *t* test). In addition, TPPU did not influence performance in the OFT (Fig. 2*E*,*F*,*K*,*L*; $t_{(25)} = 0.4462$, $p = 0.6593$ (Fig. 2*E*); $t_{(25)} = 0.9121$, $p = 0.3704$ (Fig. 2*F*); $t_{(22)} = 0.1208$, $p = 0.9049$ (Fig. 2*K*); $t_{(22)} = 0.9123$, $p = 0.3715$; unpaired *t* test (Fig. 2*L*)]. These observations indicate that sEH in the CeA is required for regulation of anxiety-related behaviors.

Because of the limitations of the pharmacological study, we next bilaterally injected AAV-*Ephx2*-shRNA into the CeA of adult C57BL/6J mice (Fig. 3*A*). Western blot analysis indicate that the sEH level in the CeA was significantly reduced in sEH knock-down (refer to as sEH-KD) mice ($t_{(10)} = 2.572$, $p = 0.0278$, unpaired *t* test; Fig. 3*B*). The sEH-KD mice showed shorter duration of open-arm exploration in the EPM and a longer latency to feed during NSF [time in the open arm, $t_{(26)} = 2.666$, $p = 0.013$, time in the closed arm, $t_{(26)} = 2.638$, $p = 0.0139$ (Fig. 3*C*); $t_{(26)} = 2.502$, $p = 0.019$; unpaired *t* test (Fig. 3*D*)] compared with control mice. sEH-KD mice showed no difference on food consumption and performance in the OFT [Fig. 3*E*–*G*; $t_{(26)} = 1.246$, $p = 0.224$ (Fig. 3*E*); $t_{(27)} = 0.6703$, $p = 0.5084$ (Fig. 3*F*); $t_{(27)} = 0.5522$, $p = 0.5853$ (Fig. 3*G*); unpaired *t* test].

To further determine whether sEH in neurons is required for anxiety-related behaviors, we selectively deleted neural sEH in the CeA of adult *Ephx2*$^{loxp/loxp}$ mice by bilateral injection of AAV-hSyn-Cre virus (Fig. 4*A*). Western blot analysis showed that sEH protein levels were markedly decreased in sEH conditional knockout (cKO)

mice ($t_{(8)}$ = 2.46, p = 0.0393, unpaired t test; Fig. 4*B*). The cKO mice exhibited significantly decreased duration of open-arms exploration in the EPM and increased latency to feed in NSF [time in the open arm, $t_{(20)}$ = 2.625, p = 0.0162, time in the closed arm, $t_{(20)}$ = 1.997, p = 0.0596 (Fig. 4*C*); $t_{(20)}$ = 2.447, p = 0.0238 (Fig. 4*D*); unpaired t test], while there were no difference in food consumption and performance in the OFT between the two groups [$t_{(20)}$ = 1.496, p = 0.1504 (Fig. 4*E*); $t_{(24)}$ = 0.2382, p = 0.8138 (Fig. 4*F*); $t_{(24)}$ = 0.09,818, p = 0.9226 (Fig. 4*G*); unpaired t test].

To examine whether astrocytic sEH also play a role in regulation of anxiety, we bilaterally injected AAV-gfaABC1D-cre virus into the CeA of *Ephx2*$^{loxp/loxp}$ mice. We found that deletion of sEH in astrocytes in the CeA showed little effects on latency to feed in the NSF, duration of open-arm exploration in the EPM, or center time in the OFT [Fig. 4*H–M*; time in the open arm, $t_{(19)}$ = 0.6195, p = 0.5429, time in the closed arm, $t_{(19)}$ = 0.7746, p = 0.4481 (Fig. 4*I*); $t_{(19)}$ = 0.06,975, p = 0.9451 (Fig. 4*J*); $t_{(19)}$ = 0.2226, p = 0.8262 (Fig. 4*K*); $t_{(16)}$ = 1.859, p = 0.0815 (Fig. 4*L*); $t_{(16)}$ = 0.07747, p = 0.9392 (Fig. 4*M*); unpaired t test], suggesting a dispensable role of astrocytic sEH in the CeA for regulation of anxiety-related behaviors. Altogether, these observations demonstrate that neuronal but not astrocytic sEH in the CeA is critical for regulation of anxiety-related behaviors.

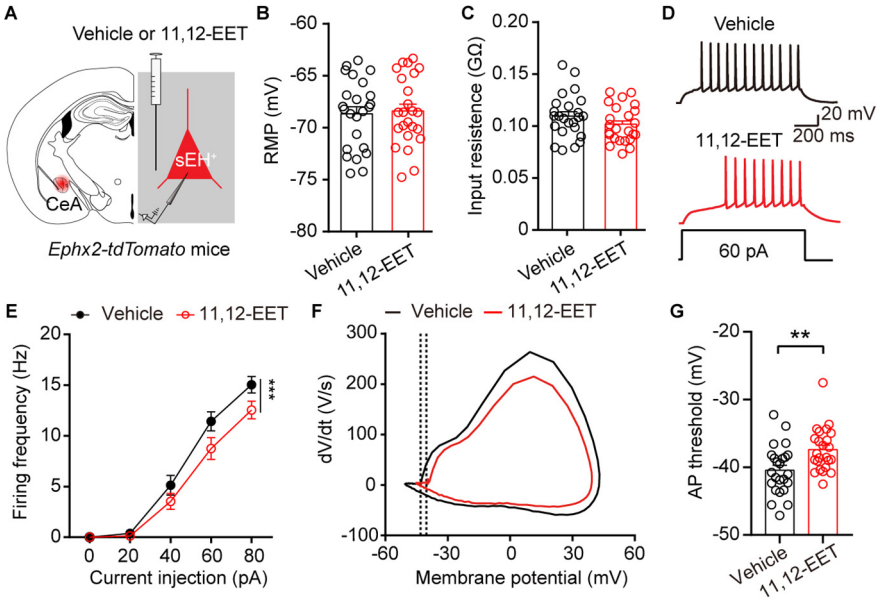

Figure 7. The intrinsic excitability of sEH-positive neurons in the CeA is decreased after application 11,12-EET. ***A***, Schematic of *in vitro* slice recording in CeA *Ephx2*-tdTomato neurons administration with 11,12-EET or vehicle. ***B***, ***C***, Resting membrane potential and input resistance recorded from *Ephx2*-tdTomato neurons treated with the 11,12-EET or vehicle. Two-tailed unpaired Student's t test, $t_{(46)}$ = 0.2598, p = 0.7961 (***B***); $t_{(46)}$ = 1.435, p = 0.1581 (***C***; n = 24 cells from 4 mice). ***D***, ***E***, Representative traces of AP responses (***D***) and summarized data (***E***) recorded from *Ephx2*-tdTomato-positive neurons administered 11,12-EET or vehicle. Two-way ANOVA, effect of drug $F_{(1,230)}$ = 9.578, $^{**}p$ = 0.0022. ***F***, Phase plots of APs from sEH-positive neurons evoked by brief current injections. ***G***, Plot diagram summary of the AP thresholds from sEH-positive neurons. Two-tailed unpaired Student's t test, $t_{(46)}$ = 3.075, $^{**}p$ = 0.0035 < 0.01 (n = 24 cells from 4 mice). Data are presented as the mean ± SEM NS ≥ 0.05; $^{*}p \leq 0.05$, $^{***}p \leq 0.001$, $^{****}p \leq 0.0001$.

sEH mediates the excitability of sEH-positive neurons in the CeA

To address how the sEH in CeA neurons modulates anxiety-related behaviors, we measured the excitability of sEH^{CeA} neurons of *Ephx2-tdTomato* mice by electrophysiological whole-cell recording (Fig. 5*A*). While TPPU treatment showed little effects on the resting membrane potential (RMP) or input resistance of sEH^{CeA} neurons [$t_{(28)}$ = 0.02999, p = 0.9763 (Fig. 5*B*); $t_{(28)}$ = 1.467, p = 0.1534 (Fig. 5*C*); unpaired t test], the firing frequencies of sEH^{CeA} neurons in response to gradually increased current injections were decreased in TPPU group compared with those in vehicle group (Fig. 5*D* and 5*E*, 5*E*, drug factor, $F_{(1,140)}$ = 5.115, p = 0.0253; two-way ANOVA). Further analysis indicated that the firing threshold of the first action potential (AP) was elevated by TPPU treatment (Fig. 5*F*,*G*, $t_{(28)}$ = 2.098, p = 0.0451; unpaired t test). On the other hand, TPPU treatment showed no effects on sEH-negative neurons [Fig. 5*H–N*; $t_{(20)}$ = 0.8129, p = 0.4258 (Fig. 5*I*); $t_{(20)}$ = 0.8345, p = 0.4139 (Fig. 5*J*); $t_{(22)}$ = 0.5923, p = 0.5597 (Fig. 5*N*), unpaired t test; drug factor, $F_{(1,100)}$ = 0.2981, p = 0.5863 (Fig. 5*L*); two-way ANOVA]. These results suggest inhibition of sEH reduces the excitability of sEH^{CeA} neurons in a cell-autonomous manner.

To further examine the role of sEH in regulation of neuronal excitability, we injected AAV-*Ephx2*-eGFP-shRNA or control virus into *Ephx2-tdTomato* mice (Fig. 6*A*). The firing frequencies were substantially decreased in sEH^{CeA} neurons infected with *Ephx2-shRNA*, with no change on RMP or input resistance, when compared with those in sEH^{CeA} neurons infected with *control-shRNA* [Fig. 6*B–E*; $t_{(25)}$ = 0.4312, p = 0.67 (Fig. 6*B*); $t_{(25)}$ = 0.7377, p = 0.4676 (Fig. 6*C*), unpaired t test; virus factor, $F_{(1,125)}$ = 25.84, p = 0.000 (Fig. 6*E*); two-way ANOVA]. Moreover, The sEH^{CeA} neurons from *Ephx2-shRNA* mice had a more depolarized firing threshold in comparison with those from *control-shRNA* mice (Fig. 6*F*,*G*, $t_{(24)}$ = 2.126, p = 0.044, unpaired t test). Again, there were no difference in sEH-negative neurons between *Ephx2-shRNA* and *control-shRNA* mice [Fig. 6*H–N*; $t_{(22)}$ = 0.8001, p = 0.4322 (Fig. 6*I*); $t_{(22)}$ = 1.078, p = 0.2929 (Fig. 6*J*); $t_{(22)}$ = 0.7389, p = 0.4678 (Fig. 6*N*), unpaired t test; virus factor, $F_{(1,110)}$ = 0.5096, p = 0.4768 (Fig. 6*L*); two-way ANOVA]. These data emphasized the indispensable role of sEH in regulation of excitability of sEH^{CeA} neurons.sEH is a key enzyme of the ARA-EET pathway that catalyzes the degradation of EETs. It has been reported that 11,12-EET substantially reduced the excitability of CA1 pyramidal cells (Mule et al., 2017). To test whether 11,12-EET play a role in regulation of the excitability of sEH^{CeA} neurons, we recorded the firings of sEH^{CeA} neurons in *Ephx2-tdTomato* mice (Fig. 7*A*). 11,12-EET (2 μM) treatment significantly reduced the firing frequencies with no effects on RMP or input resistance [Fig. 7*B–E*; $t_{(46)}$ = 0.2598, p = 0.7961 (Fig. 7*B*); $t_{(46)}$ = 1.435, p = 0.1581 (Fig. 7*C*), unpaired t test; drug factor, $F_{(1,230)}$ = 9.578, p = 0.0022 (Fig. 7*E*); two-way ANOVA]. We further analyzed the shape of AP and found that the sEH^{CeA} neurons in the 11,12-EET treatment group had a more depolarized firing threshold compared with neurons in the vehicle treatment group (Fig. 7*F*,*G*, $t_{(46)}$ = 3.075, p = 0.0035, unpaired t test). These data suggest that 11,12-EET inhibits the excitability of sEH^{CeA} neurons through elevation of firing threshold.

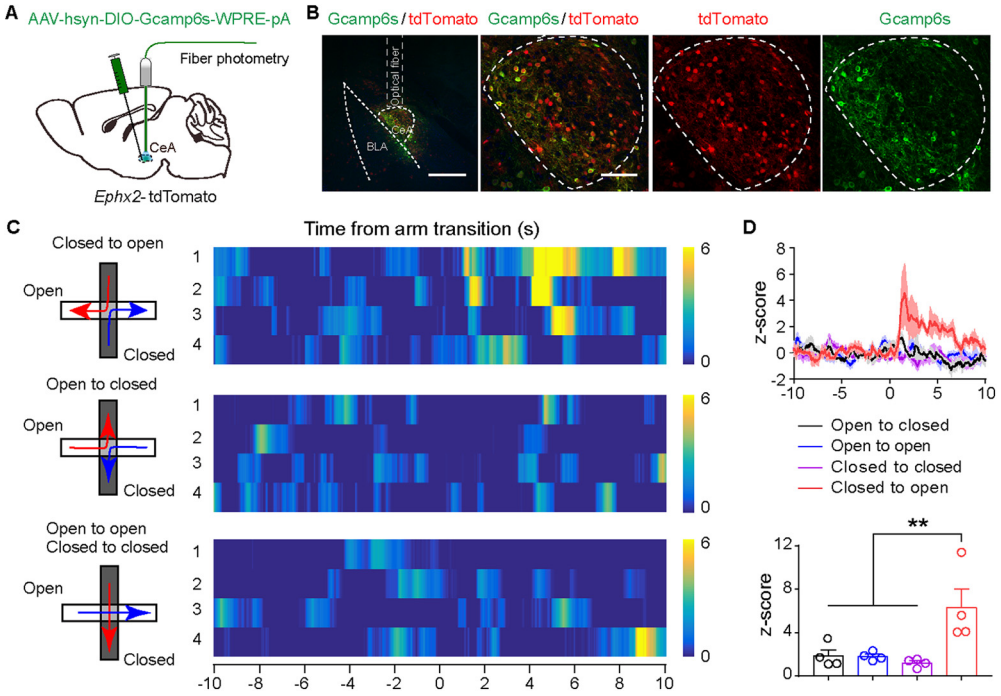

Figure 8. The activity of CeA^{sEH} neurons is associated with anxiety-related behaviors. ***A***, Optic fiber placement and virus used for fiber photometry. ***B***, Example micrographs showing the optical fiber track above the *Ephx2*-tdTomato and GCaMP6s double-positive neurons (left). Scale bar: 250 μm. Magnified images of GCaMP6s expression in the sEH-positive neurons of the CeA (right). Scale bar: 200 μm. ***C***, left, Heatmaps of normalized Ca^{2+} activity during those trajectories. Right, Example behavioral trajectories between arm compartments. ***D***, A line graph of average changes (top) and statistics of maximum changes (bottom) in normalized Ca^{2+} activity during trajectories between arm compartments. One-way ANOVA with Bonferroni *post hoc* tests, $F_{(3,12)} = 6.466$, $^{**}p = 0.0075 < 0.01$. Data are presented as the mean ± SEM NS ≥ 0.05; $^{*}p \leq 0.05$, $^{***}p \leq 0.001$, $^{****}p \leq 0.0001$.

The activity of CeA^{sEH} neurons is associated with anxiety-related behaviors

To determine whether the activity of sEH^{CeA} neurons is associated with anxiety, we performed cell-type-specific fiber photometry during exploration of innately anxiogenic environments in the EPM. AAV-hSyn-DIO-GCaMP6s virus was injected into the CeA of *Ephx2-tdTomato* mice and a fiber was implanted above the infected cells (Fig. 8*A*). This strategy resulted in the expression of GCaMP6s in sEH^{CeA} neurons (Fig. 8*B*). We compared the GCaMP6 signals of sEH^{CeA} neurons across successive behavioral entrances and exploration bouts of the arms in the EMP. The activity of sEH^{CeA} neurons was significantly increased when mice entered the open arm from closed arm, but not the open arm to open arm, open arm to closed arm or closed-arm to closed-arm (Fig. 8*C*,*D*; $F_{(3,12)} = 6.466$, $p = 0.0075$; one-way ANOVA). These findings suggest that the activity of CeA^{sEH} neurons may be involved in regulation of anxiety-related behaviors.

Bidirectional manipulations of the activity of sEH^{CeA} neurons in regulation of anxiety-related behaviors

To define the role of the activity of sEH^{CeA} neurons in anxiety-related behaviors, we bidirectionally injected the AAV-hSyn-DIO-hM3D(Gq)-mCherry virus into the CeA of *Ephx2-iCreER^{T2}* mice to specifically manipulate the activity of sEH^{CeA} neurons (Fig. 9*A*,*B*). Confocal images showed that hM3Dq was expressed in sEH^{CeA} neurons (Fig. 9*C*). Electrophysiologically, the CNO (1 μM) significantly induced firing in hM3Dq-expressing sEH^{CeA} neurons (Fig. 9*D*). We found that intraperitoneal injection of CNO (2 mg kg^{-1}) significantly increased the duration of open-arm exploration in the EPM, reduced the latency to feed without altering the food consumption in the NSF when compared with those in saline group [time in the open arm, $t_{(27)} = 2.321$, $p = 0.0281$, time in the closed arm, $t_{(27)} = 3.564$, $p = 0.0014$ (Fig. 9*E*); $t_{(23)} = 3233$, $p = 0.0037$ (Fig. 9*F*); $t_{(23)} = 0.3377$, $p = 0.7387$ (Fig. 9*G*); unpaired *t* test]. CNO had little effect on the performance in the OFT ($t_{(23)} = 0.6932$, $p = 0.4951$; unpaired *t* test; Fig. 9*H*). These data suggest that activation of sEH^{CeA} neurons produced an anxiolytic effect. In contrast, when we expressed hM4Di virus (AAV-hSyn-DIO-hM4D(Gi)-mCherry) into the CeA of *Ephx2-iCreER^{T2}* mice (Fig. 9*I*), CNO significantly inhibited the firing of sEH^{CeA} neurons (Fig. 9*J*). Behaviorally, intraperitoneal injection of CNO dramatically reduced the duration of open-arm exploration in the EPM and increased the latency to feed without altering food consumption in the NSF, whereas it had little effect on the performance in the OFT [time in the open arm, $t_{(12)} = 2.731$, $p = 0.0182$, time in the closed arm, $t_{(12)} = 1.671$, $p = 0.1206$ (Fig. 9*K*); $t_{(18)} = 2.191$, $p = 0.0419$ (Fig. 9*L*); $t_{(18)} = 1.004$, $p = 0.3289$ (Fig. 9*M*); $t_{(24)} = 1.321$, $p = 0.1989$ (Fig. 9*N*); unpaired *t* test]. These results demonstrate the critical role of the activity of sEH^{CeA} neurons in regulation of anxiety-related behaviors.

Outputs of sEH^{CeA} neurons and characterization of BNST-projecting CeA neurons

To investigate the circuitry mechanism underlying theeffects of sEH^{CeA} neurons on anxiety-related behaviors, we traced the axonal projections of sEH^{CeA}neurons by injection of the AAV2/9-Ef1α-DIO-EYFP-WPRE-pA virus into the CeA of *Ephx2-iCreER^{T2}* mice with fMOST system (OE-bio, Co, Ltd.).We observed a dense EYFP signal in the BNST, and a moderate signal in the substantia nigra pars lateralis (SNL) regions (Movie 1), implicating the existence of projection pathways from sEH^{CeA} neurons to BNST and SNL. This is further verified by injecting AAV-hSyn-FLEX-mGFP-2A-Synaptophysin-mRuby

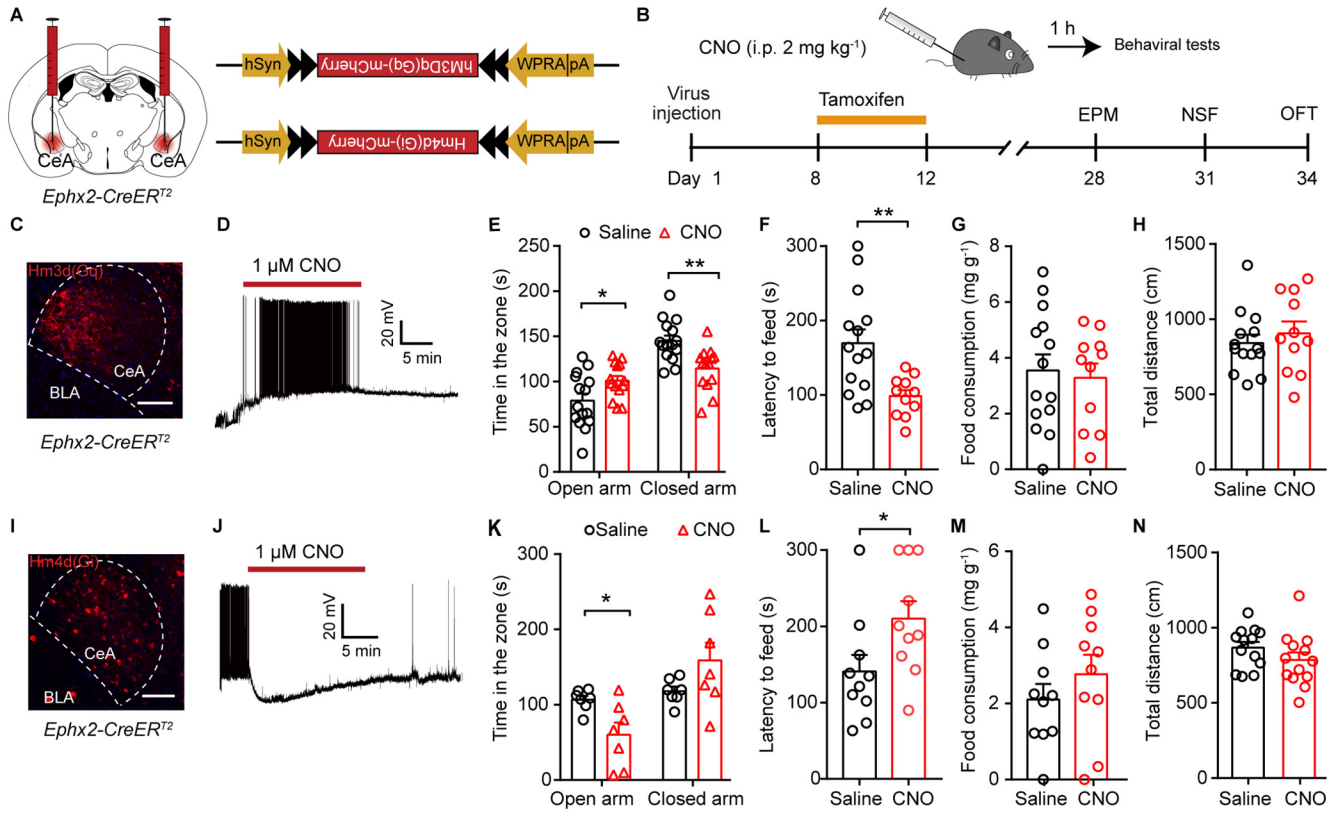

Figure 9. Bidirectional manipulations of the activity of sEH^{CeA} neurons in regulation of anxiety-related behaviors. ***A***, Stereotaxic infusion of AAV-hSyn-DIO-hM3D(Gq)-mCherry or AAV-hSyn-DIO-hM4D(Gi)-mCherry virus into the CeA of *Ephx2-iCreER^{T2}* mice with intraperitoneal injection of CNO (2 mg kg^{-1}) to regulate neural activity. ***B***, Schematic of virus injection, drug administration and behavior tests. ***C***, hM3Dq-mCherry expression in sEH-positive neurons of the CeA. Scale bar: 100 μm. ***D***, Representative traces of whole-cell recording in an acute slice from CeA sEH-positive neurons expressing hM3Dq-mCherry after bath application of 1 μM CNO. ***E***, ***G***, Chemogenetic activation of sEH-positive neurons during EPM and NSF. Time in the open arm, $t_{(27)} = 2.321$, $^{*}p = 0.02821 < 0.05$; time in the closed arm, $t_{(27)} = 3.564$, $^{**}p = 0.0014 < 0.05$ ($n = 15$ for saline, $n = 14$ for CNO; ***E***); $t_{(23)} = 3.233$, $^{**}p = 0.0037 < 0.01$ (***F***); $t_{(23)} = 0.338$, $p = 0.7387 > 0.05$ ($n = 14$ for saline, $n = 11$for CNO; ***G***). ***H***, Chemogenetic activation of sEH-positive neurons during OFT. $t_{(23)} = 0.6932$, $p = 0.4951 > 0.05$, $n = 14$ for saline, $n = 11$for CNO. ***I***, hM4Di-mCherry expression in sEH-positive neurons of the CeA. Scale bar: 100 μm. ***J***, Representative traces of whole-cell recording in an acute slice from CeA sEH-positive neurons expressing hM4Di-mCherry after bath application of 1 μM CNO. ***K–M***, Chemogenetic inhibition of sEH-positive neurons during EPM and NSF. Time in the open arm, $t_{(12)} = 2.731$, $^{*}p = 0.0182 < 0.05$; time in the closed arm, $t_{(12)} = 1.671$, $p = 0.1206$ (***K***); $t_{(18)} = 2.191$, $^{*}p = 0.0419 < 0.01$ (***L***); $t_{(18)} = 1.004$, $p = 0.3289 > 0.05$ (***M***). ***N***, Chemogenetic inhibition of sEH-positive neurons during OFT. $t_{(24)} = 1.321$, $p = 0.1989 > 0.05$. Data are presented as the mean ± SEM. Two-tailed unpaired Student's *t* test, NS ≥ 0.05; $^{*}p \leq 0.05$, $^{***}p \leq 0.001$, $^{****}p \leq 0.0001$.

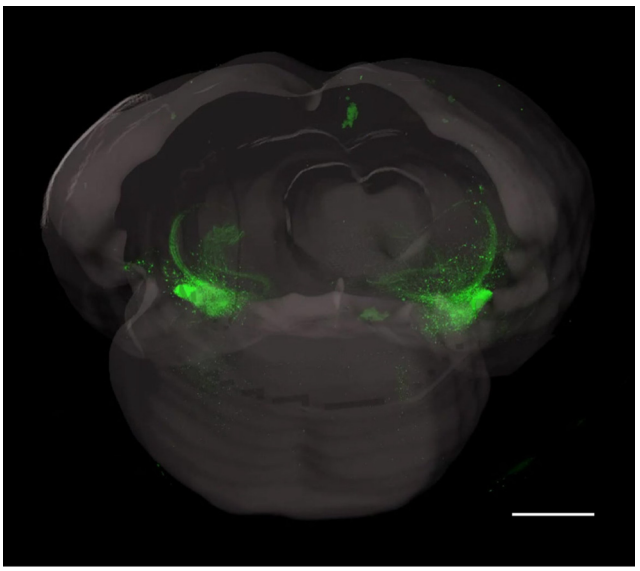

Movie 1. Visualization of 3D reconstruction for the outputs of sEH^{CeA} neurons. ***A***, The mouse brain is from the *Ephx2-iCreER ^{T2}* mice with CeA injection of AAV2/9-Ef1α-DIO-EYFP-WPRE-pA virus. Scale bars: 1500 μm. [View online]

virus, which is capable of indicating the terminal of projections, into the CeA of *Ephx2-iCreER^{T2}* mice (Fig. 10*A*). As shown in Figure 10*B*, there was a dense signal of both mCherry and GFP in the BNST and SNL (Fig. 10*B*; Extended Data Fig. 10-1*A*). Together, these results demonstrate that sEH^{CeA} neurons directly project to BNST and SNL. There were no obvious fluorescence signals in other brain regions (Extended Data Fig. 10-1*B–E*). While, it is known that the BNST is also strongly implicated in maladapted anxiety disorder (Kim et al., 2013; Marcinkiewcz et al., 2016). We mainly focused on the circuit of sEH$^{CeA\text{-}BNST}$. To determine which population of sEH^{CeA} neurons project to BNST, we back-labeled sEH^{CeA}neurons that projected to BNST by injecting AAV2-Retro-Ef1α-DIO-EYFP virus into the BNST of *Ephx2-creER^{T2}* mice (Fig. 10*C*), and co-stained with CRF, SOM, and PKCδ antibodies (Fig. 10*D–F*). As shown in Figure 9*G*, 47.2% of sEH$^{CeA\text{-}BNST}$ neurons co-labeled PKCδ, and 19.7% co-labeled CRF. There was no colocalization between sEH$^{CeA\text{-}BNST}$ and SOM (Fig. 10*G*).

Optogenetic manipulation of the sEH$^{CeA\text{-}BNST}$ circuit bidirectionally governs anxiety-related behaviors

To test the functional role of sEH$^{CeA\text{-}BNST}$ neuronal pathway in anxiety, we bilaterally injected ChR2-eYFP (AAV2/9-Ef1α-DIO-hChR2(H134R)-EYFP-WPRE-pA) or eYFP (AAV2/9-Ef1α-DIO- -EYFP-WPRE-pA) virus into the CeA of *Ephx2-iCreER^{T2}*

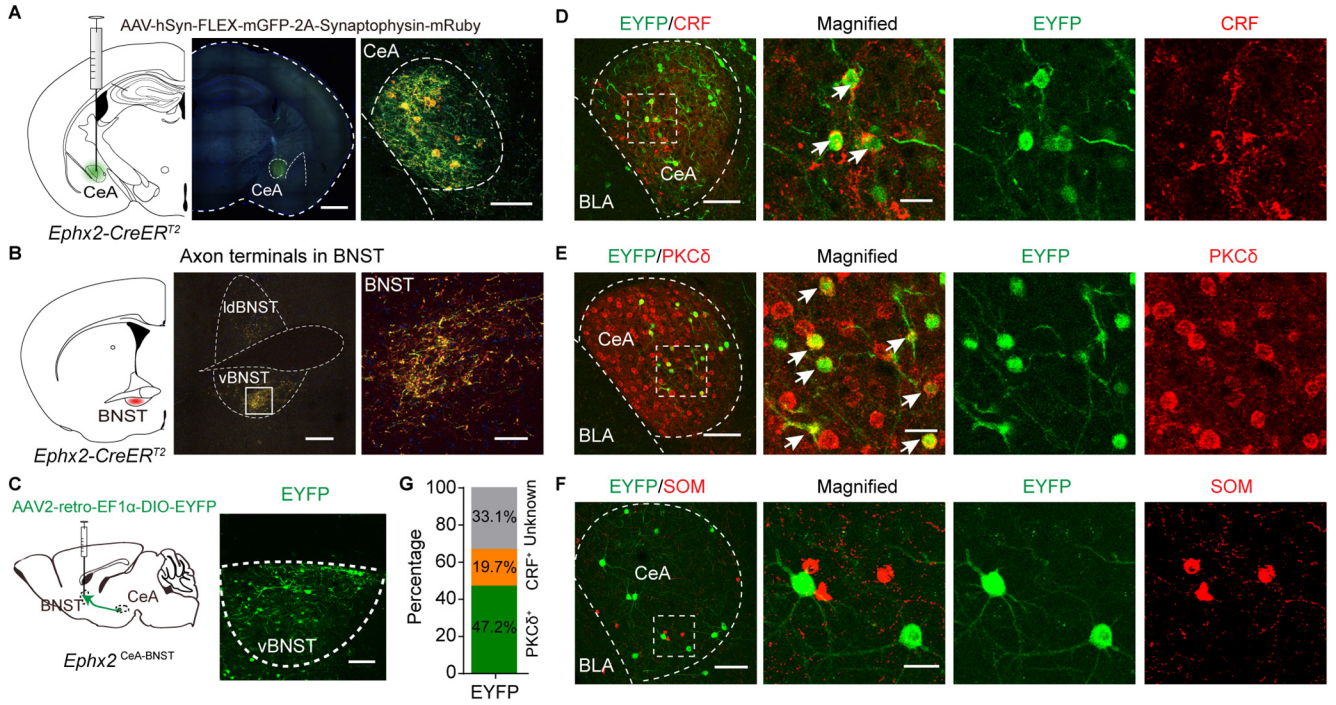

Figure 10. Outputs of sEH^{CeA} neurons and characterization of BNST-projecting CeA neurons. ***A***, Representative images of AAV-hSyn-FLEX-mGFP-2A-Synaptophysin-mRuby tracing virus expression in the sEH-positive neurons of the CeA. Scale bars: 1000 μm (left) and 50 μm (right). ***B***, Representative images of sEH-positive neurons in the CeA projection to the BNST. Scale bars: 250 μm (left) and 50 μm (right). ***C***, Representative images of AAV2-Retro-Ef1α-DIO-EYFP into the BNST of *Ephx2-creER*^{T2} mice. Scale bar: 100 μm. ***D***, Representative images of sEH^{CeA} neurons projection to BNST co-localized with CRF immunofluorescence. Scale bars: 100 μm (left) and 25 μm (right). ***E***, Representative images of sEH^{CeA} neurons projection to BNST co-localized with PKCδ immunofluorescence. Scale bars: 100 μm (left) and 25 μm (right). ***F***, Representative images of sEH^{CeA} neurons projection to BNST co-localized with SOM immunofluorescence. Scale bars: 100 μm (left) and 25 μm (right). ***G***, Quantitative analyses of sEH positive neurons in the CeA projection to the BNST co-labeled with the CRF, PKCδ, and SOM using immunostaining ($n = 649$ sEH^{+} neurons in CeA projection to BNST from 3 mice). For the images of sEH^{CeA} neurons projected to other brain regions, please refer to Extended Data Figure 10-1.

mice. An optic fiber was inserted above the BNST to allow for the delivery of blue (470 nm) light to the axons in the BNST (Fig. 11*A*). Confocal images showed dense expression of ChR2 protein on sEH^{CeA} neurons and axon terminals in the BNST (Fig. 11*B*). We performed optogenetic modulation of the sEH$^{CeA\text{-}BNST}$ circuit in the EPM, NSF, and OFT. Results showed that, while mice spent similar time in open-arm during OFF epoch, light stimulation of the sEH$^{CeA\text{-}BNST}$ circuit significantly increased the duration of open-arm exploration in ChR2 mice than that in eYFP mice (Fig. 11*C*,*D*; virus factor, $F_{(1,42)} = 4.21$, $p = 0.0465$, Bonferroni's multiple comparisons test, ON, $p = 0.0222$; two-way ANOVA). These observations suggest that activation of sEH$^{CeA\text{-}BNST}$ pathway elicits an anxiolytic effect. Note that, we failed to detect an effect of optogenetic stimulation in the ChR2 mice in the OFT and NSF [virus factor, $F_{(1,48)} = 0.3762$, $p = 0.5425$, Bonferroni's multiple comparisons test, ON, $p = 0.9999$ (Fig. 11*E*); virus factor, $F_{(1,48)} = 1.21$, $p = 0.2767$, Bonferroni's multiple comparisons test, ON, $p = 0.9999$ (Fig. 11*F*); interaction, $F_{(2,45)} = 0.4544$, $p = 0.6377$, Bonferroni's multiple comparisons test, ON, $p = 0.946$ (Fig. 11*G*); two-way ANOVA].

To examine whether inhibition of sEH$^{CeA\text{-}BNST}$ pathway could induce anxiety-like behaviors, we expressed NpHR (AAV2/9-Ef1α-DIO-eNpHR3.0-mCherry-WPRE-pA) or mCherry (AAV2/9-Ef1α-DIO-mCherry-WPRE-pA) virus in the CeA of *Ephx2-iCreER*^{T2} mice along with a bilaterally implanted optical fiber over the BNST to inhibit the sEH$^{CeA\text{-}BNST}$ pathway (Fig. 11*H*,*I*). The yellow light (580 nm) was constantly delivered during ON epoch. We found that the latency to feed was significantly increased without changes on food consumption on optogenetic inhibition of sEH$^{CeA\text{-}BNST}$ circuit in NpHR mice [Fig. 11*J*–*L*; virus factor, $F_{(1,40)} = 11.07$, $p = 0.0019$, Bonferroni's multiple comparisons test, ON, $p = 0.0115$ (Fig. 11*K*); virus factor, $F_{(1,40)} = 0.1215$, $p = 0.7293$, Bonferroni's multiple comparisons test, ON, $p = 0.7792$ (Fig. 11*L*); two-way ANOVA]. In contrast, there was little effect of optogenetic inhibition of sEH$^{CeA\text{-}BNST}$ circuit in the EPM and OFT [virus factor, $F_{(1,45)} = 0.7892$, $p = 0.3791$, Bonferroni's multiple comparisons test, ON, $p = 0.6679$ (Fig. 11*M*); virus factor, $F_{(1,57)} = 0.1363$, $p = 0.7134$, Bonferroni's multiple comparisons test, ON, $p = 0.9999$ (Fig. 11*N*); two-way ANOVA]. Nevertheless, these observations suggest that the sEH$^{CeA\text{-}BNST}$ circuit is critical for regulation of anxiety-related behaviors.

Discussion

Our study defines the neural mechanisms by which molecularly defined CeA neurons modulate anxiety-related behaviors. First, inhibition or specific deletion of sEH in CeA neurons promotes anxiety-like behaviors, which may be because of downregulated excitability of sEH^{CeA} neurons. Second, the activity of sEH^{CeA} neurons is corelated with anxiety-related behaviors, and chemogenetic manipulations of the activity of sEH^{CeA} neurons bidirectionally regulate anxiety-related behaviors. Last, sEH^{CeA} neurons mainly project to BNST, and optogenetic manipulations of the sEH$^{CeA\text{-}BNST}$ circuit are sufficient to affect anxiety-related behaviors. Together, these data support a model in which the activity of sEH^{CeA} neurons leads to anxiety-related behaviors via both molecular and long-range circuit mechanisms.sEH has been reported to mostly localize in astrocytes throughout the brain. Using *Ephx2*-tdTomato mice and sEH antibody, we demonstrate that sEH is also expressed in neurons in the CeA (Fig. 1), in line with a previous study (Marowsky et al., 2009). By using multiple approaches, including pharmacology, AAV-shRNA and

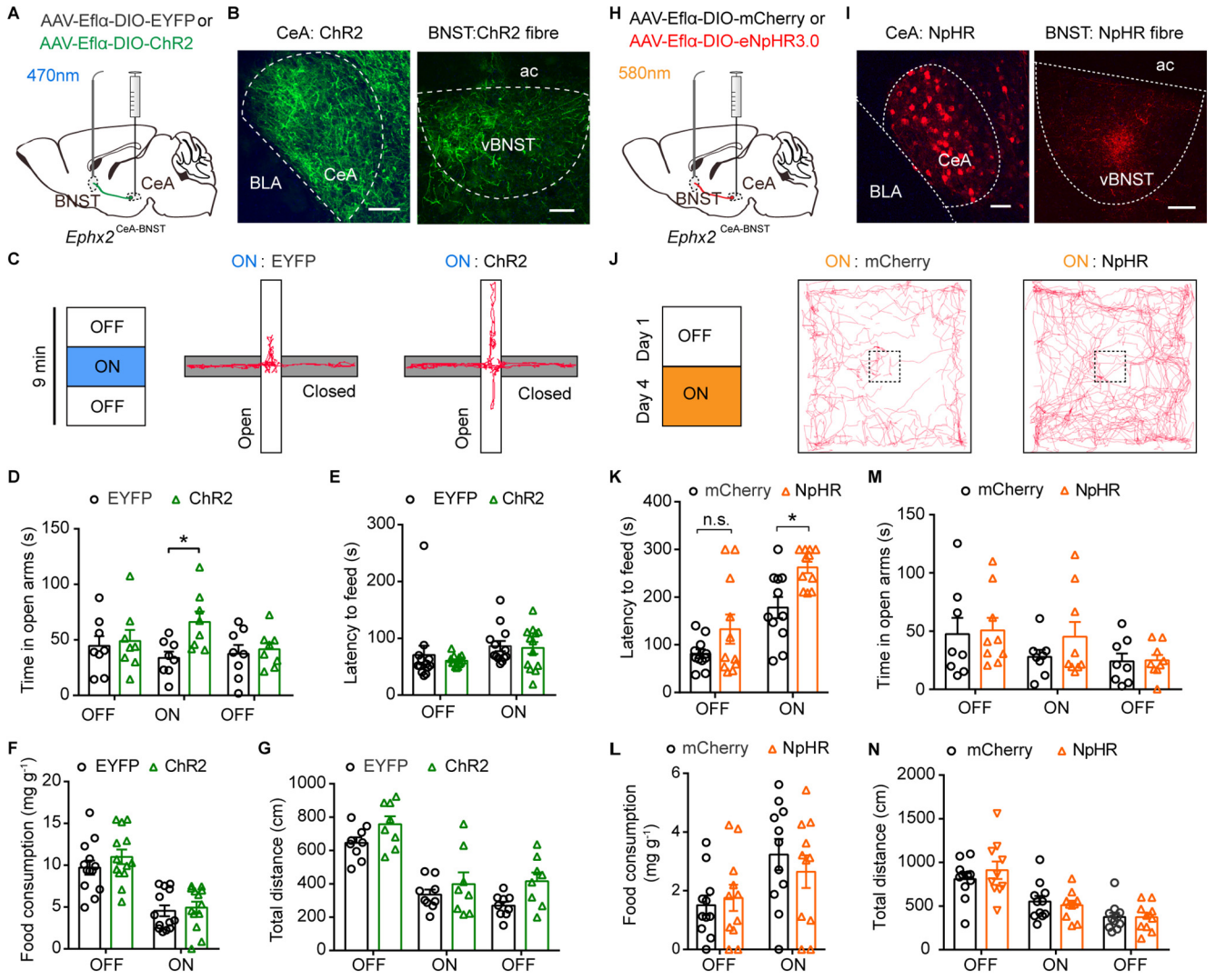

Figure 11. Optogenetic manipulations of the sEH $^{CeA\text{-}BNST}$ circuit bidirectionally regulate anxiety-related behaviors. ***A***, Schematic of virus injection to express ChR2. ***B***, Images of chR2 expression in the sEH-positive neurons of the CeA and projection to the BNST. Scale bars: 100 μm (left) and 25 μm (right). ***C***, left, Three-minute epochs across the 9-min session. Right, Representative animal track for the middle epochs of EPM for an EYFP-mouse and chR2-mouse. ***D***, Optogenetic activation of the CeA-BNST pathway during EPM. Two-way ANOVA, effect of virus, $F_{(1,42)} = 4.21$, $^{*}p = 0.0465$. ***E***, ***F***, Optogenetic activation of sEH$^{CeA-BNST}$ pathway during the NSF. Two-way ANOVA, effect of virus, $F_{(1,48)} = 0.3762$, $p = 0.5425$ (***E***); $F_{(1,48)} = 1.21$, $p = 0.2767$ (***F***). ***G***, Optogenetic activation of the CeA-BNST pathway during the OFT. Two-way ANOVA, effect of virus, $F_{(1,45)} = 8.882$, $^{**}p = 0.0046$. ***H***, Schematic of virus injection to express NpHR. ***I***, Images of NpHR expression in the sEH-positive neurons of the CeA and projection to the BNST. Scale bars: 50 μm (left) and 100 μm (right). ***J***, left, Schematic of the experimental design. Right, Representative tracks of NSF for mCherry and NpHR mice. ***K***, ***L***, The latency to feed and food consumption during NSF with optogenetic inhibition of the CeA-BNST pathway. Two-way ANOVA, effect of virus, $F_{(1,40)} = 11.07$, $^{**}p = 0.0019$ (***K***); $F_{(1,40)} = 0.1215$, $p = 0.7293$ (***L***). ***M***, Optogenetic inhibition of sEH$^{CeA-BNST}$ pathway during the EPM. Two-way ANOVA, effect of virus, $F_{(1,45)} = 0.7892$, $p = 0.3791$. ***N***, Optogenetic inhibition of sEH$^{CeA-BNST}$ pathway during the OFT. Two-way ANOVA, effect of virus, $F_{(1,57)} = 0.1363$, $p = 0.7134$. Data are presented as the mean ± SEM NS ≥ 0.05; $^{*}p \leq 0.05$, $^{***}p \leq 0.001$, $^{****}p \leq 0.0001$.

condition knock-out, we find that sEH in neurons in the CeA is required for anxiety-like behaviors (Figs. 2-4). One recent study showed that sEH−/− mice displayed anxiety-like behaviors without clear molecular and neural circuit mechanisms (Lee et al., 2019). Together, these findings demonstrated a novel role for sEH in the regulation of anxiety and might extend the function of the ARA-EET pathway in the brain.

What are the molecular mechanisms underlying the modulation of anxiety by sEH? sEH is a key enzyme of the ARA-EET pathway that catalyzes the degradation of EETs. In the electrophysiology experiments, we find that the sEH inhibitor TPPU and AAV-Ephx2-shRNA decreased the excitability of sEH^{CeA} neurons (Figs. 5, 6). Notably, 11,12-EET, which could be degraded by sEH, also exhibited suppressive effect on the excitability of sEH^{CeA} neurons (Fig. 7), in consistent with a previous report (Mule et al., 2017). It is plausible to speculate that sEH may regulate the excitability of sEH^{CeA} neurons via 11,12-EET. However, the detailed mechanisms need to be further studied.

The identification of neuronal subpopulations in the CeA that positively regulate anxiety has long remained elusive. In our study, chemogenetic and optogenetic manipulations of the sEH^{CeA} neurons and sEH$^{CeA-BNST}$ circuit bidirectionally regulate anxiety-related behaviors. It is noteworthy that while chemogenetic manipulations exhibited regulative effects in both the EPM and NSF, whereas optogenetic manipulations only showed effect either in the EPM (activation of sEH$^{CeA-BNST}$ circuit) or in the NSF (inhibition of sEH$^{CeA-BNST}$ circuit). These different behavioral outcomes between chemogenetic manipulation and optogenetic manipulation studies might be because of the different methods used and/or the different subtypes of

neurons manipulated. Note that, except BNST, sEH^{CeA} neurons also send projections to other regions such as SNL (Extended Data Fig. 10-1). The behavioral outcomes of the chemogenetic manipulations of sEH^{CeA} neurons, which theoretically activate all the projecting pathways, may be incompletely consistent with those of optogenetic manipulations of $sEH^{CeA-BNST}$ pathway specifically.

The CeA has been reported to comprises distinct neuronal populations of inhibitory GABAergic neurons that express CRF, SOM, or PKCδ (Fadok et al., 2017), which partly co-stained with sEH (17.6 $\pm$ 5.5%, 31.6 $\pm$ 5.8%, and 25.3 $\pm$ 5.1%, respectively). We find that sEH partly colocalizes with CRF, SOM, and PKCδ at rate of 17.6 $\pm$ 5.5%, 31.6 $\pm$ 5.8%, and 25.3 $\pm$ 5.1%, respectively. Previous studies have shown that CRF-expressing neurons in the CeA that project to the ventral tegmental area (VTA) or BNST regulate anxiety (Dedic et al., 2018). We describe a new population of sEH-expressing cells in the CeA that innervate the BNST, which is required for regulation of anxiety-related behaviors (Figs. 8-11). Nevertheless, the functions of sEH^{CeA} neurons that project to other brain regions, such as SNL, and the mechanisms underlying the regulation of anxiety-like behaviors warranted further investigation.

References

Ahrens S, Wu MV, Furlan A, Hwang GR, Paik R, Li H, Penzo MA, Tollkuhn J, Li B (2018) A central extended amygdala circuit that modulates anxiety. J Neurosci 38:5567–5583.

Atone J, Wagner K, Hashimoto K, Hammock BD (2020) Cytochrome P450 derived epoxidized fatty acids as a therapeutic tool against neuroinflammatory diseases. Prostaglandins Other Lipid Mediat 147:106385.

Bazinet RP, Layé S (2014) Polyunsaturated fatty acids and their metabolites in brain function and disease. Nat Rev Neurosci 15:771–785.

Bi LL, Sun XD, Zhang J, Lu YS, Chen YH, Wang J, Geng F, Liu F, Zhang M, Liu JH, Li XW, Mei L, Gao TM (2015) Amygdala NRG1-ErbB4 is critical for the modulation of anxiety-like behaviors. Neuropsychopharmacology 40:974–986.

Birn RM, Shackman AJ, Oler JA, Williams LE, McFarlin DR, Rogers GM, Shelton SE, Alexander AL, Pine DS, Slattery MJ, Davidson RJ, Fox AS, Kalin NH (2014) Evolutionarily conserved prefrontal-amygdalar dysfunction in early-life anxiety. Mol Psychiatry 19:915–922.

Calhoon GG, Tye KM (2015) Resolving the neural circuits of anxiety. Nat Neurosci 18:1394–1404.

Dedic N, Kühne C, Jakovcevski M, Hartmann J, Genewsky AJ, Gomes KS, Anderzhanova E, Pöhlmann ML, Chang S, Kolarz A, Vogl AM, Dine J, Metzger MW, Schmid B, Almada RC, Ressler KJ, Wotjak CT, Grinevich V, Chen A, Schmidt MV, et al. (2018) Chronic CRH depletion from GABAergic, long-range projection neurons in the extended amygdala reduces dopamine release and increases anxiety. Nat Neurosci 21:803–807.

Fadok JP, Krabbe S, Markovic M, Courtin J, Xu C, Massi L, Botta P, Bylund K, Müller C, Kovacevic A, Tovote P, Lüthi A (2017) A competitive inhibitory circuit for selection of active and passive fear responses. Nature 542:96–100.

Gilpin NW, Herman MA, Roberto M (2015) The central amygdala as an integrative hub for anxiety and alcohol use disorders. Biol Psychiatry 77:859–869.

Griessner J, Pasieka M, Böhm V, Grössl F, Kaczanowska J, Pliota P, Kargl D, Werner B, Kaouane N, Strobelt S, Kreitz S, Hess A, Haubensak W (2021) Central amygdala circuit dynamics underlying the benzodiazepine anxiolytic effect. Mol Psychiatry 26:534–544.

Harris TR, Hammock BD (2013) Soluble epoxide hydrolase: gene structure, expression and deletion. Gene 526:61–74.

Haubensak W, Kunwar PS, Cai H, Ciocchi S, Wall NR, Ponnusamy R, Biag J, Dong HW, Deisseroth K, Callaway EM, Fanselow MS, Lüthi A, Anderson DJ (2010) Genetic dissection of an amygdala microcircuit that gates conditioned fear. Nature 468:270–276.

Huang Y, Wang Y, Wang H, Liu Z, Yu X, Yan J, Yu Y, Kou C, Xu X, Lu J, Wang Z, He S, Xu Y, He Y, Li T, Guo W, Tian H, Xu G, Xu X, Ma Y, et al. (2019) Prevalence of mental disorders in China: a cross-sectional epidemiological study. Lancet Psychiatry 6:211–224.

Kalin NH, Shelton SE, Davidson RJ (2004) The role of the central nucleus of the amygdala in mediating fear and anxiety in the primate. J Neurosci 24:5506–5515.

Kim HW, Rapoport SI, Rao JS (2011) Altered arachidonic acid cascade enzymes in postmortem brain from bipolar disorder patients. Mol Psychiatry 16:419–428.

Kim SY, Adhikari A, Lee SY, Marshel JH, Kim CK, Mallory CS, Lo M, Pak S, Mattis J, Lim BK, Malenka RC, Warden MR, Neve R, Tye KM, Deisseroth K (2013) Diverging neural pathways assemble a behavioural state from separable features in anxiety. Nature 496:219–223.

Lee HT, Lee KI, Lin HC, Lee TS (2019) Genetic deletion of soluble epoxide hydroxylase causes anxiety-like behaviors in mice. Mol Neurobiol 56:2495–2507.

Lemos JC, Wanat MJ, Smith JS, Reyes BA, Hollon NG, Van Bockstaele EJ, Chavkin C, Phillips PE (2012) Severe stress switches CRF action in the nucleus accumbens from appetitive to aversive. Nature 490:402–406.

Lin R, Wang R, Yuan J, Feng Q, Zhou Y, Zeng S, Ren M, Jiang S, Ni H, Zhou C, Gong H, Luo M (2018) Cell-type-specific and projection-specific brain-wide reconstruction of single neurons. Nat Methods 15:1033–1036.

Marcinkiewcz CA, Mazzone CM, D'Agostino G, Halladay LR, Hardaway JA, DiBerto JF, Navarro M, Burnham N, Cristiano C, Dorrier CE, Tipton GJ, Ramakrishnan C, Kozicz T, Deisseroth K, Thiele TE, McElligott ZA, Holmes A, Heisler LK, Kash TL (2016) Serotonin engages an anxiety and fear-promoting circuit in the extended amygdala. Nature 537:97–101.

Marowsky A, Burgener J, Falck JR, Fritschy JM, Arand M (2009) Distribution of soluble and microsomal epoxide hydrolase in the mouse brain and its contribution to cerebral epoxyeicosatrienoic acid metabolism. Neuroscience 163:646–661.

Mnookin S (2016) Out of the shadows: making mental health a global development priority. Washington, DC: World Bank Group. Available at https://documents.worldbank.org/en/publication/documents-reports/documentdetail/270131468187759113/out-of-the-shadows-makingmental-health-a-global-development-priority.

Mocking RJ, Ruhé HG, Assies J, Lok A, Koeter MW, Visser I, Bockting CL, Schene AH (2013) Relationship between the hypothalamic-pituitary-adrenal-axis and fatty acid metabolism in recurrent depression. Psychoneuroendocrinology 38:1607–1617.

Morisseau C, Hammock BD (2013) Impact of soluble epoxide hydrolase and epoxyeicosanoids on human health. Annu Rev Pharmacol Toxicol 53:37–58.

Mule NK, Orjuela Leon AC, Falck JR, Arand M, Marowsky A (2017) 11,12 -Epoxyeicosatrienoic acid (11,12 EET) reduces excitability and excitatory transmission in the hippocampus. Neuropharmacology 123:310–321.

Nery FG, Monkul ES, Hatch JP, Fonseca M, Zunta-Soares GB, Frey BN, Bowden CL, Soares JC (2008) Celecoxib as an adjunct in the treatment of depressive or mixed episodes of bipolar disorder: a double-blind, randomized, placebo-controlled study. Hum Psychopharmacol 23:87–94.

Onorati M, Castiglioni V, Biasci D, Cesana E, Menon R, Vuono R, Talpo F, Laguna Goya R, Lyons PA, Bulfamante GP, Muzio L, Martino G, Toselli M, Farina C, Barker RA, Biella G, Cattaneo E (2014) Molecular and functional definition of the developing human striatum. Nat Neurosci 17:1804–1815.

Pomrenze MB, Tovar-Diaz J, Blasio A, Maiya R, Giovanetti SM, Lei K, Morikawa H, Hopf FW, Messing RO (2019) A corticotropin releasing factor network in the extended amygdala for anxiety. J Neurosci 39:1030–1043.

Purves KL, Coleman JRI, Meier SM, Rayner C, Davis KAS, Cheesman R, Bækvad-Hansen M, Børglum AD, Wan Cho S, Jürgen Deckert J, Gaspar HA, Bybjerg-Grauholm J, Hettema JM, Hotopf M, Hougaard D, Hübel C, Kan C, McIntosh AM, Mors O, Bo Mortensen P, et al. (2020) A major role for common genetic variation in anxiety disorders. Mol Psychiatry 25:3292–3303.

Ren Q, Ma M, Ishima T, Morisseau C, Yang J, Wagner KM, Zhang JC, Yang C, Yao W, Dong C, Han M, Hammock BD, Hashimoto K (2016) Gene

deficiency and pharmacological inhibition of soluble epoxide hydrolase confers resilience to repeated social defeat stress. Proc Natl Acad Sci USA 113:E1944–E1952.

Scott-Van Zeeland AA, Bloss CS, Tewhey R, Bansal V, Torkamani A, Libiger O, Duvvuri V, Wineinger N, Galvez L, Darst BF, Smith EN, Carson A, Pham P, Phillips T, Villarasa N, Tisch R, Zhang G, Levy S, Murray S, Chen W, et al. (2014) Evidence for the role of EPHX2 gene variants in anorexia nervosa. Mol Psychiatry 19:724–732.

Tovote P, Fadok JP, Lüthi A (2015) Neuronal circuits for fear and anxiety. Nat Rev Neurosci 16:317–331.

Tye KM, Prakash R, Kim SY, Fenno LE, Grosenick L, Zarabi H, Thompson KR, Gradinaru V, Ramakrishnan C, Deisseroth K (2011) Amygdala circuitry mediating reversible and bidirectional control of anxiety. Nature 471:358–362.

Wan D, Yang J, McReynolds CB, Barnych B, Wagner KM, Morisseau C, Hwang SH, Sun J, Blocher R, Hammock BD (2019) In vitro and in vivo metabolism of a potent inhibitor of soluble epoxide hydrolase, 1-(1-propionylpiperidin-4-yl)-3-(4-(trifluoromethoxy)phenyl)urea. Front Pharmacol 10:464.

World Health Organization (2017) Depression and other common mental disorders: global health estimates. Available at https://www.who.int/publications/i/item/depression-global-health-estimates.

Xiong W, Cao X, Zeng Y, Qin X, Zhu M, Ren J, Wu Z, Huang Q, Zhang Y, Wang M, Chen L, Turecki G, Mechawar N, Chen W, Yi G, Zhu X (2019) Astrocytic epoxyeicosatrienoic acid signaling in the medial prefrontal cortex modulates depressive-like behaviors. J Neurosci 39:4606–4623.